3 Phenomenological decoherence and dissipation

Decoherence is understood as suppression of quantum mechanical interference effects and consequently, the transition from microscopic coherent quantum behavior to classical macroscopic physical behavior. Various mesoscopic systems such as quantum dots, nanowires and macroscopic coherent systems, for example quantum Hall systems, superfluids or superconductors at low temperatures exihibit quantum behavior, on the other hand many phenomena at room temperature can be explained from classical laws of physics. In this chapter, we discuss several aspects of decoherence in the context of charge transport in ordered and disordered electrical conductors and Aharonov-Bohm (AB) interferometer. In the previous chapter, we have introduced and developed the Langevin equations and Green's functions (LEGF) approach in the context of heat conduction. Similar formalism has also been developed for quantum charge transport in mesoscopic systems [31, 32]. Here, first, we employ the LEGF method to study decoherence phenomena in ordered one dimensional chain [65] in Sec.(3.1) and AB interferometer [84] in Sec.(3.2) through phenomenologial voltage probes. As discussed in Chapter (1), the voltage probe acts as a source of inelastic scattering and as a result, introduces both decoherence and dissipation in the system. Later, in Sec.(3.3), we introduce random-phase reservoir [85], which gives rise to localization instead of decoherence. We also explicitly illustrate the comparison between random-phase reservoir and voltage probes. Then, in Sec.(3.4), we extend the phenomenology of decoherence via stochastic absorption in higher dimensions using Migdal-Kadanoff type scaling argument [86]. We apply the invariant embedding approach to the last two problems.

The quantity of fundamental interest in theoretical and experimental study of decoherence in metals and semiconductors is the electron dephasing time, τ_ϕ. Several experiments [87] observing quantum interference, such as weak localization in films and wires, universal conductance fluctuations in disordered quantum wires, AB oscillations and persistent currents in mesoscopic rings show decoherence. At finite temperature, the main source of decoherence in metals and semiconductors is inelastic e-ph scattering. In three dimensional weakly disordered conductors, e-ph scattering is the sole dominant inelastic dephasing process. For strongly disordered conductors, e-e scattering dominates over the e-ph scattering rate near the mobility edge. At low temperatures (T) in metals and semiconductors, small-energy-transfer (quasielastic) e-e scattering (with

dephasing time τ_{ee}) is the dominant dephasing process. In these systems, in two dimensions, $1/\tau_{ee} \sim T$, while in one dimension, $1/\tau_{ee} \sim T^{2/3}$. It can be understood as the interaction of an electron with the fluctuating electromagnetic field produced by all the other electrons, i.e., dephasing by the equilibrium Nyquist noise. One of the most debated issue in this field is the saturation of τ_ϕ at very low temperatures, which has been observed in experiment. This is still an open question with many arguments, for example extrinsic mechanisms like magnetic spin-spin scattering, electromagnetic noise sources or nonequilibrium effects, and intrinsic mechanisms such as the effect of e-e interaction or interaction between conduction electrons and dynamical defects. In this chapter, we do not explicitly calculate τ_ϕ, instead, we are interested to see the consequence of decoherence on the transport behavior in ordered and disordered conductors, metallic rings and on the metal-insulator Anderson transition.

3.1 Inelastic scattering via voltage probes in ordered wires

Inelastic scattering provides a mechanism for dissipation and decoherence in quantum systems. These effects are important in understanding transport properties of mesoscopic systems. Experimental examples are numerous, namely studies of transport in systems such as single walled carbon nanotubes [88], atomic chains [89, 90], semiconducting heterostructures [91] and polymer nanofibers [92]. In the absence of inelastic scattering, transport is either ballistic and we see effects such as conductance quantization [6, 7], or, with elastic scatterers, we see effects of coherent scattering such as Anderson localization [93]. In either case, transport is non-Ohmic, even when we consider very long wires. Introducing inelastic scattering necessarily leads to decoherence and both of the above effects (ballistic transport, localization) are reduced. One expects that in the limit of long wires, one should get Ohmic transport [94]. Recent experiments on atomic chains [95] and Fullerene bridges [96, 97] have studied the effects of inelastic scattering and the associated local heating on quantum transport.

The physical sources for inelastic scattering are well known; they occur due to the interaction of the conducting electrons with other degrees of freedom in the system. However, the microscopic modeling of inelastic scattering in the context of transport is nontrivial. One of the first phenomenological models for dissipation was due to Büttiker [24, 25]. In Büttiker's model, one connects a point inside the wire to a reservoir of electrons maintained at a chemical potential μ whose value is set by the condition that there is no average current flow into this side reservoir. This is equivalent to connecting a voltage probe at some point on the wire, and a nice experimental realization of this situation can be seen in [91]. In Büttiker's model, an electron flowing into the reservoir can emerge with a different phase and energy and thus one can have both decoherence and dissipation.

A more detailed microscopic calculation using Büttiker's idea of incorporating inelastic scattering was performed by D'Amato and Pastawski [98]. In their study, they considered transmission across a wire modeled by the tight-binding Hamiltonian with a nearest-neighbour hopping parameter V. Each site on the wire is connected to electron baths which are themselves modeled by tight-binding Hamiltonians with hopping parameter η. The wire is attached at the two ends to ideal leads with the same hopping parameter as the wire. These two leads are connected to reservoirs kept at fixed chemical potentials μ_L and μ_R for the left and right leads, respectively. The side leads are attached to reservoirs whose chemical potentials are fixed self-consistently by imposing the condition of zero current. Using this model, D'Amato and Pastawski analytically solved the case where the self-energy correction due to the side leads is purely imaginary and has the form $i\eta$, where η is small. They were able to demonstrate the transition from coherent to Ohmic transport. An inelastic length scale $\ell = aV/\eta$, with a as a lattice parameter, was introduced such that for wire length $L << \ell$, transport was coherent while for $L >> \ell$, transport was Ohmic. A number of other papers [99–101] have also shown that other models of inelastic scattering, for example, those due to e-ph (using side reservoirs as ensemble of harmonic oscillators to describe the heat bath) or e-e interactions, can be related to the Büttiker mechanism. Some recent papers have looked at e-ph interactions using the Keldysh nonequilibrium Green's function formalism combined with density-functional methods [102], tight-binding molecular-dynamics [103] and the self-consistent Born approximation [104]. An alternative mechanism for introducing inelastic scattering, through introduction of an imaginary potential in the Hamiltonian, has also been studied [105–108].

Here we present an extension of the work of D'Amato and Pastawski. We study the case of transport of both heat and electron in the presence of inelastic scatterers in the form of self-consistent leads. The wire is subjected to both chemical potential and temperature gradients and we evaluate steady state values of both the particle and heat current operators. In the limit of a long wire when one is in the Ohmic regime we are able to obtain explicit expressions for all the linear response coefficients. It is verified that various linear response results such as Onsager reciprocity and the Weidemann-Franz law are valid. In the intermediate regime between ballistic and Ohmic transport we propose a simple model of right moving and left moving persistent random walkers which can explain much of the observed behaviour. We also perform an explicit calculation of the heat loss along the wire. This is a second order effect in the gradients and we show that there is uniform heat dissipation along the length of the wire whose value is precisely the Joule heat loss. For short wires we show that heat dissipation takes place primarily at the contacts. While heat dissipation by Büttiker probes has been discussed in [25, 109], we believe that this is the first explicitly microscopic calculation of dissipation in a quantum wire that clearly demonstrates Joule heat loss in the Ohmic regime and dissipation into the reservoirs in the ballistic regime. The formalism used here is the quantum-LEGF approach. Thus apart from extending

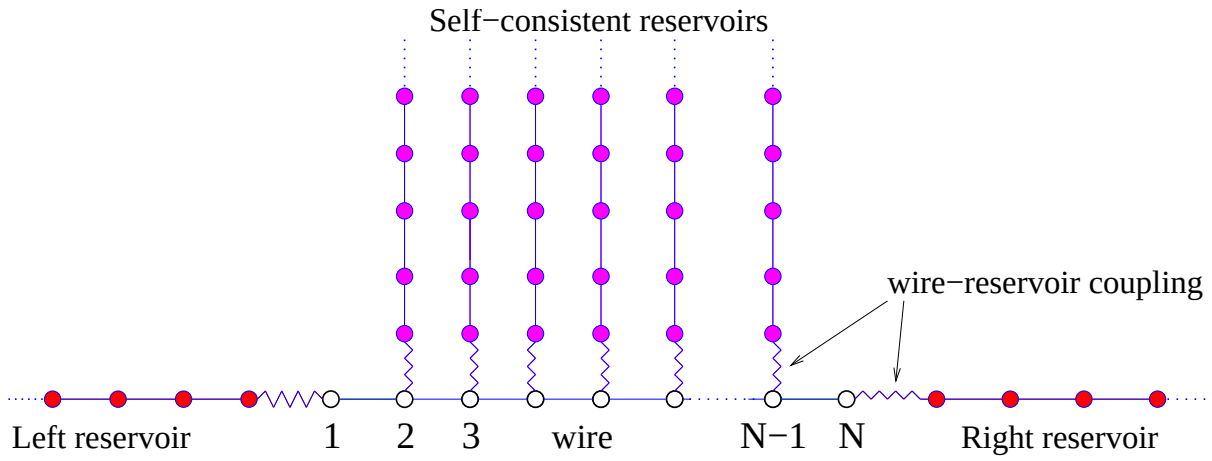

FIGURE 3.1: A schematic description of the model.

the results of [98] we also use a different and more general approach. Unlike [98] we also consider large values of the inelasticity parameter.

3.1.1 Model and general results

We consider a one-dimensional wire modeled by the tight-binding lattice Hamiltonian. The wire has N sites each of which is coupled to an infinite reservoir which is itself modeled by a one-dimensional tight-binding system [see Fig. (3.1)]. The Hamiltonian of the system consisting of the wire and all the reservoirs is given by

$$\begin{aligned} \mathcal{H} &= \mathcal{H}_W + \sum_{l=1}^{N} \mathcal{H}_R^l + \sum_{l=1}^{N} \mathcal{V}_{WR}^l \\ \text{where} \quad \mathcal{H}_W &= -\sum_{l=1}^{N-1} \gamma \, (c_l^\dagger c_{l+1} + c_{l+1}^\dagger c_l) \\ \mathcal{H}_R^l &= -\gamma_l \sum_{\alpha=1}^{\infty} (c_\alpha^{l\dagger} c_{\alpha+1}^l + c_{\alpha+1}^{l\dagger} c_\alpha^l) \qquad l = 1, 2..N \\ \mathcal{V}_{WR}^l &= -\gamma_l' \, (c_1^{l\dagger} c_l + c_l^\dagger c_1^l) \qquad l = 1, 2...N \; . \end{aligned} \tag{3.1}$$

Here c_l and c_α^l denote respectively operators on the wire and on the l^{th} reservoir. The Hamiltonian of wire is denoted by $\mathcal{H}_W$, that of the l^{th} reservoir by $\mathcal{H}_R^l$ and the coupling between the wire and the l^{th} site is $\mathcal{V}_{WR}^l$. The coupling between the reservoirs and the wire is controlled by the parameters γ_l'.

We briefly indicate the steps leading to generalized quantum Langevin equations of motion for the wire variables. We assume that for $t \leq t_0$ the reservoirs are disconnected from the wire. Each

reservoir is in equilibrium at a specified temperature T_l and chemical potential μ_l. At time t_0 we connect all the reservoirs to the wire and we are interested in the steady state properties of the wire. For $t > t_0$, the Heisenberg equations of motion for the wire and reservoirs variables are:

$$\dot{c}_l = \frac{i\gamma}{\hbar}(c_{l-1} + c_{l+1}) + \frac{i\gamma'_l}{\hbar}c_1^l \quad \text{for } \; l = 1, 2...N \; , \tag{3.2}$$

$$\dot{c}_\alpha^l = \frac{i\gamma_l}{\hbar}(c^l{}_{\alpha-1} + c^l{}_{\alpha+1}) \quad \text{for} \quad \alpha = 2, 3, ...\infty \; , \;\; l = 1, 2, ...N \tag{3.3}$$

$$\dot{c}_1^l = \frac{i\gamma_l}{\hbar}c_2^l + \frac{i\gamma'_l}{\hbar}c_l \quad \text{for } \; l = 1, 2...N \tag{3.4}$$

and we have taken $c_0 = c_{N+1} = 0$. The equation of motion of the wire variables Eq. (3.2) involves the reservoir variable c_1^l and we will try to eliminate this. We note that the equation of motion of each of the N reservoirs, given by Eq. (3.3,3.4), is a set of linear equations with an inhomogeneous part given by $i\gamma'_l c_l/\hbar$. We can solve these equations of motion using the single particle Green's function of the reservoirs which is given by $g^l(t) = -i\theta(t)e^{-iH^l t/\hbar}$ where H^l is the single-particle Hamiltonian of the l^{th} reservoir. We finally find that the solution for the boundary site on the l^{th} reservoir is given by (for $t > t_0$)

$$c_1^l(t) = i\sum_{\alpha=1}^{\infty} g_{1\alpha}^{l+}(t - t_0)c_\alpha^l(t_0) - \int_{t_0}^{\infty} dt' \; g_{1,1}^{l+}(t - t') \; \frac{\gamma'_l}{\hbar} \; c_l(t') \tag{3.5}$$

Plugging this into the equation of motion Eq. (3.2) of wire variables, we get

$$\dot{c}_l(t) = \frac{i\gamma}{\hbar}(c_{l-1} + c_{l+1}) - i\eta_l - i\int_{t_0}^{\infty} dt' \Sigma_l^+(t - t')c_l(t') \tag{3.6}$$

$$\text{where} \quad \eta_l(t) = -\frac{i\gamma'_l}{\hbar} \; \sum_{\alpha=1}^{\infty} g_{1\alpha}^{l+}(t - t_0) \; c_\alpha^l(t_0)$$

$$\Sigma_l^+(t) = (\frac{\gamma'_l}{\hbar})^2 \; g_{1,1}^{l+}(t)$$

This is in the form of a generalised quantum Langevin equation where we identify η_l as noise from the l^{th} reservoir and the last term in Eq. (3.6) is the dissipative term. The noise depends on the reservoir's initial distribution which we have chosen to be an equilibrium distribution. The properties of the noise is written most conveniently in the frequency domain. We consider the limit $t_0 \to -\infty$. Let us define the Fourier transforms $\tilde{c}_l(\omega) = (1/2\pi)\int_{-\infty}^{\infty} dt e^{i\omega t}c_l(t)$, $g^{l+}(\omega) = \int_{-\infty}^{\infty} dt e^{i\omega t}g^{l+}(t)$, $\tilde{\eta}_l(\omega) = (1/2\pi) \; \int_{-\infty}^{\infty} dt e^{i\omega t}\eta_l(t)$ and $\Sigma_l^+(\omega) = (\gamma'_l/\hbar)^2 g_{1,1}^{l+}(\omega)$. Let us also use the definition $\Gamma_l(\omega) = -Im[\Sigma_l^+]/\pi = (\gamma'_l/\hbar)^2\rho_l(\omega)$ where $\rho_l(\omega)$ is the local density of states at the first site ($\alpha = 1$) on the l^{th} reservoir. With these definitions it is easy [32] to show that the noise-noise correlations are given by

$$\langle\tilde{\eta}_l^\dagger(\omega)\tilde{\eta}_m(\omega')\rangle = \Gamma_l(\omega) \; f(\omega, \; \mu_l, \; T_l) \; \delta(\omega - \omega') \; \delta_{lm} \; , \tag{3.7}$$

where $f(\omega,\mu,T) = 1/\{exp[(\hbar\omega-\mu)/k_BT]+1\}$ is the Fermi distribution function.

Taking Fourier transform of the equation of motion Eq. (3.6) we thus get the following steady state solution

$$\begin{aligned} \tilde{c}_l(\omega) &= \sum_{m=1}^{N} G^+_{lm}(\omega)\ \tilde{\eta}_m(\omega) \qquad (3.8)\\ \text{where}\quad G^+ &= \frac{\hbar}{\gamma} Z^{-1} \\ \text{and}\quad Z_{lm} &= \frac{\hbar}{\gamma}(\omega - \Sigma^+_l)\ \delta_{lm} + \delta_{l,m-1} + \delta_{l,m+1}\ . \end{aligned}$$

As shown in [32] $G^+(\omega)$ is basically the Green's function of the full system (wire and reservoirs) and for points on the wire can be written in the form $G^+(\omega) = [\omega - H_W/\hbar - \bar{\Sigma}^+]^{-1}$ where H_W is the single particle Hamiltonian of the wire while $\bar{\Sigma}^+$, defined by its matrix elements $\bar{\Sigma}^+_{lm} = \Sigma^+_l \delta_{lm}$, is a self-energy correction arising from the interaction with the reservoirs. We will be interested in particle and energy currents in the system. The corresponding operators are obtained by defining particle and energy density operators and obtaining their continuity equations [31]. The particle density is defined on sites while the energy density is defined on bonds. We will be interested in currents both inside the wire and between the wire and reservoirs. Let us define j^p_l as the particle current between sites $l\ , l+1$ on the wire and j^u_l as the energy current between the bonds $(l-1,l)$ and $(l,l+1)$. Also we define j^p_{w-l} as the particle current from the wire to the l^{th} reservoir and similarly j^u_{w-l} is the energy current from the wire to the l^{th} reservoir. These are given by the following expectation values:

$$\begin{aligned} j^p_l &= \frac{i\gamma}{\hbar}\langle\ c^\dagger_{l+1}c_l - c^\dagger_l c_{l+1}\ \rangle \\ j^u_l &= \frac{i\gamma^2}{\hbar}\langle\ c^\dagger_{l-1}c_{l+1} - c^\dagger_{l+1}c_{l-1}\ \rangle \\ j^p_{w-l} &= \frac{-i\gamma'_l}{\hbar}\langle\ c^\dagger_l c^l_1 - {c^l_1}^\dagger c_l\ \rangle \\ j^u_{w-l} &= \frac{i\gamma\gamma'_l}{\hbar}\langle\ (c^\dagger_{l+1} + c^\dagger_{l-1})\ c^l_1 - {c^l_1}^\dagger(c_{l+1}+c_{l-1})\ \rangle\ . \end{aligned}$$

Using the general solution in Eq. (3.33) and the noise properties in Eq. (3.7) we can evaluate the

above expressions and find

$$j_l^p = \sum_{m=1}^{N} \frac{-i\gamma{\gamma'_m}^2}{\hbar^3} \int_{-\infty}^{\infty} d\omega(\ G^+_{lm}G^-_{ml+1} - G^+_{l+1m}G^-_{ml}\ )\ \rho_m\ (f_l - f_m) \tag{3.9}$$

$$j_l^u = \sum_{m=1}^{N} \frac{i\gamma^2{\gamma'_m}^2}{\hbar^3} \int_{-\infty}^{\infty} d\omega(\ G^+_{l-1m}G^-_{ml+1} - G^+_{l+1m}G^-_{ml-1}\ )\ \rho_m\ (f_l - f_m) \tag{3.10}$$

$$j^p_{w-l} = \sum_{m=1}^{N} \frac{1}{2\pi} \int_{-\infty}^{\infty} d\omega \mathcal{T}_{lm}\ (f_l - f_m) \tag{3.11}$$

$$j^u_{w-l} = \sum_{m=1}^{N} \frac{1}{2\pi} \int_{-\infty}^{\infty} d\omega\ \hbar\omega\ \mathcal{T}_{lm}\ (f_l - f_m)\ , \tag{3.12}$$

where $G^-_{lm} = {G^+_{ml}}^*$ and $\mathcal{T}_{lm} = 4\pi^2\gamma'^2_l{\gamma'_m}^2\rho_l\rho_m|G^+_{lm}|^2/\hbar^4$ can be shown to be the transmission probability of a wave from the l^{th} to the m^{th} reservoir.

3.1.2 Self-consistent determination of chemical potential profile

We consider the case where the wire is held in a fixed temperature field specified by the temperatures, $T_l,\ l = 1, 2...N$, of the N reservoirs. We will consider a small temperature difference and assume that the applied temperature field has the linear form

$$T_l = T_L + \frac{l-1}{N-1}\Delta T\ ,$$

where $\Delta T = T_R - T_L$. The chemical potentials at the ends of the wire are specified by the conditions $\mu_1 = \mu_L$ and $\mu_N = \mu_R$. The $N-2$ side reservoirs $l = 2, 3...N-1$ are included to simulate other degrees of freedom present in a real wire and the requirement of zero net particle current into these reservoirs self-consistently fixes the values of their chemical potentials. Thus the chemical potentials $\{\mu_l\}$ for $l = 2, 3...N-1$ are obtained by solving the following set of $N-2$ equations:

$$j^p_{w-l} = 0 \quad \text{for} \quad l = 2, 3, ...N-1\ , \tag{3.13}$$

with j^p_{w-l} given by Eq. (3.11). Once the chemical potential profile is determined, we can use Eqs. (3.9,3.10) to determine the particle and heat currents in the system while Eq. (3.12) gives the heat exchange with the environment (side reservoirs).

In general the set of equations Eq. (3.38) are nonlinear and difficult to solve analytically. We will henceforth consider the low temperature and linear response regime where the applied chemical potential difference $\Delta\mu = \mu_R - \mu_L$ and the temperature difference ΔT are both small. More specifically we shall assume $\Delta\mu << \mu_{L,R},\ \Delta T << T_{L,R}$ and $k_B T_{L,R} << \mu_{L,R}$. For simplicity we restrict ourselves to the following choice of parameters: $\gamma_l = \gamma'_1 = \gamma'_N = \gamma$ for $l = 1, 2...N$

and $\gamma_l' = \gamma'$ for $l = 2, 3...N-1$. Thus all the reservoirs will have the same Green's function and density of states and we will use the notation $g_{1,1}^{l+}(\omega) = g^+(\omega)$ and $\rho_l(\omega) = \rho(\omega)$.

Making Taylor expansions of the Fermi functions $f(\omega, \mu_l, T_l)$ about the mean values $\mu = (\mu_L + \mu_R)/2$ and $T = (T_L + T_R)/2$, we find that, in the linear response regime, Eq. (3.38) reduces to the following set of equations:

$$j_{w-l}^p = \sum_{m=1}^{N} \frac{1}{2\pi\hbar} \left[\mathcal{T}_{lm} \, (\mu_l - \mu_m) + \frac{\pi^2 k_B^2 T}{3\hbar} \, \mathcal{T}'_{lm}(T_l - T_m) \right] = 0 \quad \text{for} \quad l = 2, 3...N-1 \,, \tag{3.14}$$

where $\mathcal{T}_{lm}$ and $\mathcal{T}'_{lm} = d\mathcal{T}_{lm}/d\omega$ are evaluated at $\omega = \mu/\hbar$. These are linear equations in $\{\mu_l\}$ and are straightforward to solve numerically. We can then use Eq. (3.9) and Eq. (3.10) to find the particle and heat current. The local heat current in the wire is given by $j_l^q = j_l^u - \mu_l j_l^p$. In the linear response regime we find

$$\begin{aligned} j_l^p &= \frac{-1}{2\pi\hbar} \sum_{m=1}^{N} [\mathcal{F}_{lm} \, (\mu_l - \mu_m) + \frac{\pi^2 k_B^2 T}{3\hbar} \mathcal{F}'_{lm} \, (T_l - T_m)] \\ j_l^q &= \frac{-1}{2\pi\hbar} \sum_{m=1}^{N} [\, \frac{\pi^2 k_B^2 T^2}{3\hbar} \mathcal{F}'_{lm} \, (\mu_l - \mu_m) + \frac{\pi^2 k_B^2 T}{3} \mathcal{F}_{lm} \, (T_l - T_m) \,] \,, \end{aligned} \tag{3.15}$$

where $\mathcal{F}_{lm} = (2\pi i \gamma \gamma'^2/\hbar^3) \, (\, G_{lm}^+ G_{ml+1}^- - G_{l+1m}^+ G_{ml}^- \,) \, \rho$ and $\mathcal{F}_{lm}, \mathcal{F}'_{lm}$ are evaluated at $\omega = \mu/\hbar$. The heat loss from the wire to the reservoir can be obtained using Eq. (3.12). As we shall see later this heat loss is a second order effect and therefore we will keep terms up to second order in the expansion. We then get

$$\begin{aligned} j_{w-l}^q = \frac{1}{2\pi\hbar} \sum_{m=1}^{N} \Bigg[& -\frac{\pi^2 k_B^2 T^2}{3\hbar} \mathcal{T}'_{lm} \, (\mu_l - \mu_m) - \frac{\pi^2 k_B^2 T}{3} \mathcal{T}_{lm} \, (T_l - T_m) \\ + \quad & \frac{1}{2} \mathcal{T}_{lm} \, (\mu_l - \mu_m)^2 + \frac{2\pi^2 k_B^2 T}{3\hbar} \, \mathcal{T}'_{lm} \, (\mu_l - \mu_m)(T_l - T_m) + \frac{\pi^2 k_B^2}{3} \, \mathcal{T}_{lm} \, (T_l - T_m)^2 \Bigg] \end{aligned} \tag{3.16}$$

In the next subsection we will the consider the case of a long wire ($N \to \infty$) and consider particle and heat transport in the presence of applied chemical potential and temperature gradients. Later, for an isothermal system, we will consider finite systems and discuss the transition from coherent to Ohmic transport.

3.1.3 Long wire with applied chemical potential and temperature gradients

Let us first evaluate the matrix elements $\mathcal{T}_{lm}(\omega)$. This involves $\rho(\omega)$ and $G_{lm}^+(\omega)$. As discussed before $\rho(\omega)$ is the local density of states at the boundary site of a semi-infinite one-dimensional chain and is given by $\rho(\omega) = (\hbar/(\pi\gamma)[1 - \hbar^2\omega^2/(4\gamma^2)]^{1/2}$ for $|\hbar\omega| < 2\gamma$ and zero elsewhere. For

lattice points in the bulk of the wire, *i.e* points which are at a distance $>> \ell = 1/\alpha_R$ from the boundaries of the wire we find (see Appendix B.1) $G^+_{lm} = (-1)^{l+m}\hbar\ e^{-|l-m|\alpha}/(2\gamma \sinh\alpha)$. We now try the following solution for the self-consistent equations given by Eq. (3.14):

$$\mu_l = \mu_L + \frac{l-1}{N-1}\Delta\mu\ . \tag{3.17}$$

Using the fact that $\sum_{m=-\infty}^{m=\infty}(l-m)\ e^{-|l-m|\alpha} = 0$, we see that the self-consistent equations are satisfied for all points l in the bulk of the wire (up to corrections which become exponentially small with the distance from the boundaries). Close to the boundaries the chemical potential variation is no longer linear. Here we focus on the limit where N is very large and the linear solution in Eq. (3.17) is accurate in the bulk of the wire.

We will now use this solution to evaluate the various currents in the wire given by Eq. (3.15) and the heat loss from Eq. (3.16). We evaluate these currents at points l in the bulk of the wire and (since G^+_{lm} decays exponentially with distance) do not need the correct form of μ_l at the boundaries. We also find, as expected, that the currents are independent of l. They have the expected linear response forms:

$$\begin{aligned} j^p &= -L_{11}\nabla\mu - L_{12}\nabla T \\ j^q &= -L_{21}\nabla\mu - L_{22}\nabla T\ , \end{aligned}$$

where $\nabla\mu = \Delta\mu/N$, $\nabla T = \Delta T/N$ and the various transport coeficients are given by

$$L_{11} = \frac{1}{2\pi\hbar}\sum_{m=-\infty}^{\infty}\mathcal{F}_{lm}(\mu/\hbar)\ (l-m) = \frac{1}{\pi\hbar}\ \frac{\sin^2\alpha_I \coth\alpha_R}{\cosh 2\alpha_R - \cos 2\alpha_I}\ , \tag{3.18}$$

$$L_{12} = \frac{\pi^2 k_B^2 T}{3}\ \frac{dL_{11}}{d\mu}\ , \tag{3.19}$$

$$L_{21} = T\ L_{12}\ , \tag{3.20}$$

$$L_{22} = \frac{\pi^2 k_B^2 T}{3}\ L_{11}\ , \tag{3.21}$$

where α_R and α_I are respectively the real and imaginary parts of α and are all calculated at $\omega = \mu/\hbar$. In deriving the above form of L_{11} we have used the relation $\rho = 2\gamma\hbar \sinh\alpha_R \sin\alpha_I/(\pi\gamma'^2)$. In the parameter regime we are looking at, it follows that both Ohm's law and Fourier's law are valid, with the electrical and thermal conductivities given by $\sigma = e^2 L_{11}$ and $\kappa = L_{22}$. We note that Eq. (3.20) gives the Onsager reciprocity relation. This is usually derived within linear response theory and follows from time reversal invariance of the microscopic equations of motion. We also find from Eq. (3.21) that the Weidemann-Franz relation is satisfied. This relation states that the ratio of the thermal conductivity and the electrical conductivity is linearly proportional to the temperature with a universal constant of proportionality given by $\pi^2 k_B^2/(3e^2)$. For metals a derivation of this relation using semiclassical tramsport theory and within the relaxation time

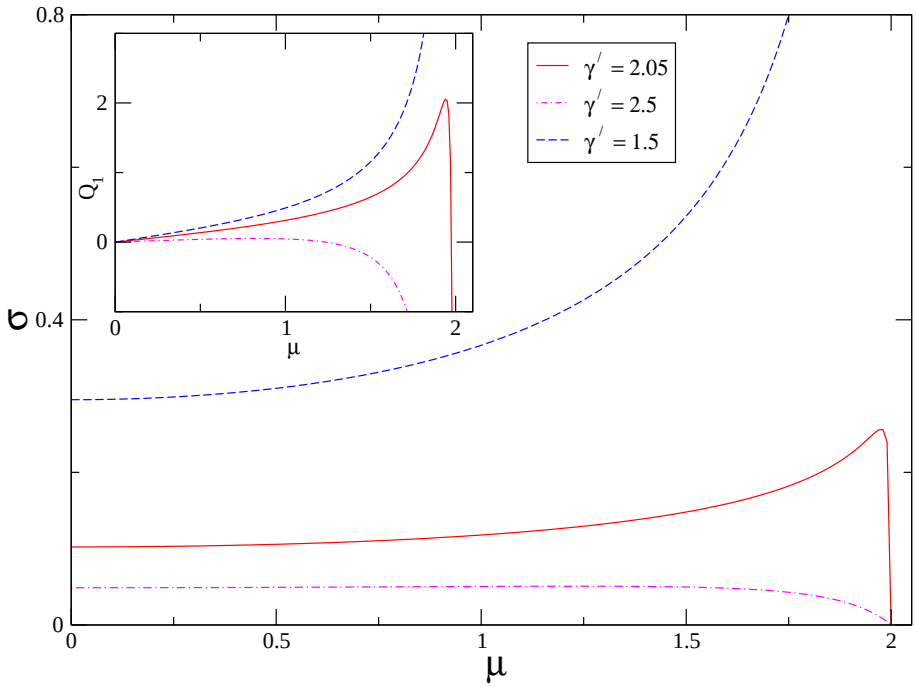

FIGURE 3.2: Plot of the conductivity and thermopower $Q_1 = 3e^2Q/(\pi^2 k_B^2 T)$ (Inset) as functions of the Fermi level μ for different values of the inelasticity parameter γ'. They are plotted in units of $e^2/\pi\hbar$ and γ respectively.

approximation can be found in [1]. The validity of this relation requires that inelastic processes can be neglected (see discussion in [1]). However we find that the relation continues to be valid in our model even though scattering is inelastic (since there is energy dissipation into the side reservoirs).

From Eq (3.19) we find that the Mott formula for the thermopower holds [110, 111]. This is given by

$$Q = \frac{L_{12}}{eL_{11}} = \frac{\pi^2 k_B^2 T}{3e} \frac{1}{\sigma} \frac{d\sigma}{d\mu} \ . \tag{3.22}$$

Recently [112] have reported an interesting resonance, arising due to electron-electron interactions, observed in the thermopower as a function of the Fermi energy. We investigate if there are any interesting features in the dependence of Q on μ in our model. In Fig (3.2) we plot the conductivity and the thermopower $3e^2Q/(\pi^2 k_B^2 T) = d(\ln\sigma)/d\mu$ as a function of μ for different values of the coupling constant γ'. Surprisingly we find that for a range of values of the inelasticity parameter γ' there is a peak in the thermopower as a function of the Fermi energy.

Let us now look at the heat exchanges given by Eq. (3.16). In the long-wire limit, the condition of zero particle currents into the side reservoirs, Eq. (3.14), implies that $\sum_m \mathcal{T}_{lm}(l-m) =$

$\sum_m \mathcal{T}'(l-m) = 0$. Hence the terms linear in $\nabla\mu$ and ∇T in Eq. (3.16) vanish, and only the second order terms contribute significantly. Let us first consider the coefficient of the term containing $(\nabla\mu)^2$ which is given by

$$\frac{1}{4\pi\hbar}\sum \mathcal{T}_{lm}\ (l-m)^2\ . \tag{3.23}$$

Evaluating the sum we find that it is exactly equal to L_{11}. Determining the other terms in Eq. (3.16) we find that the net heat loss per unit length (or from every bulk site) of the wire is given by:

$$j^q = L_{11}\ (\nabla\mu)^2 + \frac{4\pi^2 k_B^2 T}{3}\ \frac{dL_{11}}{d\mu}\ (\nabla\mu)(\nabla T) + \frac{2\pi^2 k_B^2}{3}\ L_{11}(\nabla T)^2\ . \tag{3.24}$$

The first term corresponds to the expected Joule heat loss in a wire and is always positive. The second term can be of either sign and can be identified to be the Thomson effect which corresponds to heat exchange that occurs in a wire (in addition to the Joule heat) when an electric current flows across a temperature gradient.

Finally we check for local thermal equilibrium in the wire. A requirement of local equilibrium would be that the local density n_l at the point l in the nonequilibrium state should be the same as the density n_l^{eq} at the point if the entire wire was kept in equilibrium at a chemical potential μ_l and temperature T_l. It is easy to evaluate n_l and n_l^{eq} and we find:

$$n_l - n_l^{eq} = \sum_{m=1}^{N} \frac{\gamma'^2}{\hbar^2} \int_{-\infty}^{\infty} d\omega |G^+_{lm}(\omega)|^2\ \rho(\omega)\ [\ f(\omega,\mu_m,T_m) - f(\omega,\mu_l,T_l)\ ]\ ,$$

which in the linear response regime, gives

$$n_l - n_l^{eq} = \frac{\gamma'^2}{\hbar^3}\ \sum_{m=1}^{N}\left[\ |G^+_{lm}(\mu/\hbar)|^2\ \rho(\mu/\hbar)\ (\mu_l-\mu_m) + \frac{\pi^2 k_B^2 T}{3}\ \frac{d}{d\mu}[|G^+_{lm}(\mu/\hbar)|^2\rho(\mu/\hbar)]\ (T_l - T_m)\ \right]\ .$$

For our linear profiles of temperature and chemical potential and the form of G_{lm} it is clear that, for all bulk points, the above difference vanishes (upto order $O(1/N)$). Thus we see that the local densities are consistent with the assumption of local equilibrium.

3.1.4 Current flow in wire in isothermal conditions: finite size effects

In this section we look at finite length wires. We first solve Eq. (3.14) numerically to determine the chemical potential profile and then estimate the current in the wire using Eq. (3.15). We also look at the local heat dissipation at all points on the wire.

In our numerical calculations we have chosen the parameter values $\mu_L = 1.0, \mu_R = 1.1, \gamma = 1.0$ and have considered different values of the dissipation strength γ' and different system sizes N.

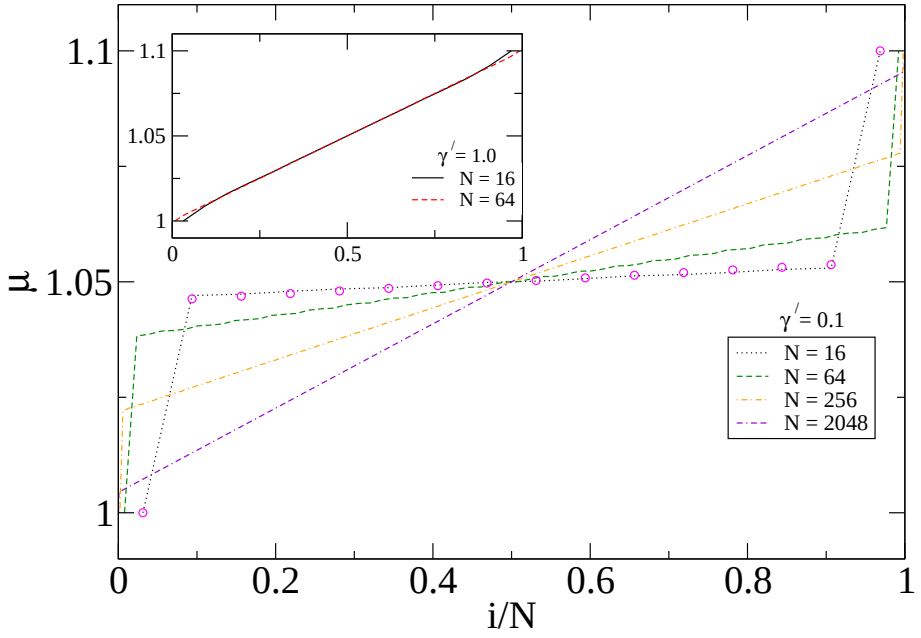

FIGURE 3.3: Plot of the chemical potential profile μ_i as a function of the scaled length i/N for different values of N and with $\gamma' = 0.1$. The points denoted by circles correspond to the approximate solution given in Eq. (3.26). The inset shows the chemical potential profile for $\gamma' = 1.0$.

In Fig. (3.3) we plot the chemical potential profile, for different system sizes, for a small value of the dissipation ($\gamma' = 0.1$). We see that as we go to larger system sizes, chemical potential profile changes, from a flat profile with large jumps at the boundaries, to a smooth linear profile. For a larger dissipation parameter ($\gamma' = 1.0$) we see [inset of Fig. (3.3)] that a smooth linear profile is obtained even for small system sizes. The limit of weak dissipation was studied in [98] . Following them we find that for $\gamma'/\gamma << 1$ a very good approximation for the transmission coefficients $\mathcal{T}_{lm}$, for any system size, is given by

$$\mathcal{T}^{+}_{lm} = \frac{\pi^2 \gamma_l'^2 \gamma_m'^2 \rho^2}{\hbar^2 \gamma^2} e^{-\frac{2|l-m|}{\ell}} \quad . \tag{3.25}$$

where $\ell = 1/\alpha_R \approx 2\gamma^2/\gamma'^2$. Note that, for $l = 2, 3, ...N-1$, $\mathcal{T}_{1l}$ and $\mathcal{T}_{lN}$ are $O(\gamma'^2)$ while $\mathcal{T}_{lm}$ for $m = 2, 3, ...N-1$ are $O(\gamma'^4)$. We then find that, for $\ell >> 1$ and $N >> 1$, the following chemical potential profile provides a good approximate solution of the self-consistent equations:

$$\begin{aligned} \mu_1 &= \mu_L, \quad \mu_N = \mu_R \\ \mu_l &= \mu_L - \delta - \frac{2\delta}{\ell}(l-2) \quad \text{for} \quad l = 2, 3, ...N-1 \\ \text{where} \quad \delta &= \frac{\mu_L - \mu_R}{2(1 + N/\ell)} \end{aligned} \tag{3.26}$$

Plugging in this solution into the self-consistency equations $\sum_m \mathcal{T}_{lm}(\mu_l - \mu_m) = 0$ with $\mathcal{T}_{lm}$ given by Eq. (3.25) we can explicitly verify that these are satisfied upto corrections of order $1/\ell$. In Fig. (3.3) we have plotted the above solution for system size $N = 16$ and find an excellent agreement with the numerical result (for larger system sizes the fit agreement becomes better).

The above solution leads to the following result for the current:

$$\frac{jN}{\Delta\mu L_{11}} = \frac{1}{1+\ell/N} \ , \tag{3.27}$$

where L_{11} is the ohmic conductivity of the wire given by Eq. (3.18) and we have normalized the current such that the $N \to \infty$ limit gives a constant value independent of γ'.

We have also looked at the transition from coherent to Ohmic transport for general values of the dissipation parameter γ'. In Fig. (3.4) we plot the scaled current $jN/(\Delta\mu L_{11})$ as a function of system size. We find that in general for any $\gamma'/\gamma < 1$ the data can be fitted quite accurately to the form in Eq. (3.55) with $\ell = 1/\alpha_R$ which can be interpreted as a coherent length scale. For $\gamma'/\gamma > 1$ we find that there is no coherent regime and the approach to the asymptotic limit has a different form.

Persistent random walk model: It is possible to understand the various aspects of the intermediate regime within a simple classical Drude-like framework of right moving and left moving electrons moving in fixed directions but with a small probability of inter-conversion. We consider the case where the left reservoir is kept at a chemical potential $\mu + \Delta\mu$ and the right reservoir is at μ. At the low temperatures being considered electron transport is basically due to the electrons close to the Fermi level and we can focus on the electrons within the energy gap $\Delta\mu$ in the left reservoir. Let the density of these electrons inside the left reservoir be $2\rho_L$ and this consists of an equal proportion of right moving electrons with velocity v_F and left movers with velocity $-v_F$. In the right reservoir the density of both left and right movers in the energy window $\Delta\mu$ is zero. Inside the wire the presence of the side-reservoirs allows a right mover to be converted to a left mover with some probability. We now present the following random walk model to incorporate the above basic idea. The model consists of a lattice of N sites with a density ρ_l^+ of right movers and ρ_l^- of left movers at all sites $l = 1, 2...N$. We impose the boundary conditions $\rho_1^+ = \rho_1^- = \rho_L$ and $\rho_N^+ = \rho_N^- = 0$. At sites $l = 2, 3...N-1$ the particles move according to the following rules: with probability p a right mover at site l moves to $l+1$ and, with probability $1-p$ it transforms to a left mover and moves to site $l-1$. Similarly, with probability p a left mover at site l moves to $l-1$ and, with probability $1-p$ it transforms to a right mover and moves to $l+1$. At sites $l = 1, N$, the right mover always moves to the right and the left mover moves to the left. It is then straightforward to write discrete time-evolution equations for the density fields $\rho_i^+(t)$ and $\rho_i^-(t)$. Choosing a lattice length scale a and a microscopic time scale τ we obtain, in the

continuum limit

$$\begin{aligned} \frac{\partial \rho^+(x,t)}{\partial t} &= -v\frac{\partial \rho^+}{\partial x} - \alpha(\rho^+ - \rho^-) \\ \frac{\partial \rho^-(x,t)}{\partial t} &= v\frac{\partial \rho^-}{\partial x} + \alpha(\rho^+ - \rho^-)\ . \end{aligned} \tag{3.28}$$

where $v = ap/\tau$ can be identified with the Fermi velocity v_F and $\alpha = (1-p)/\tau$ gives the scattering rate (Note that the continuum limit requires taking $a \to 0$, $\tau \to 0$ and $p \to 1$ keeping v and α finite). We obtain a length scale v/α which we tentatively identify with the scattering length ℓ introduced earlier. The boundary conditions for the above equations are $\rho^+(x=0) = \rho_L$ amd $\rho^-(x=L) = 0$, where $L = Na$. These give the following steady state solution for Eq. (3.28):

$$\rho(x) = \rho^+(x) + \rho^-(x) = 2\rho_L - \delta' - \frac{2\delta'}{\ell}x \tag{3.29}$$

$$\text{where} \quad \delta' = \frac{2\rho_L}{2(1+L/\ell)} \tag{3.30}$$

is the density jump at the boundaries. This immediately leads to Eq. (3.26) once we note that $\rho(x) - 2\rho_L \propto \mu_l - \mu_L$. The current in the wire is given by

$$J = v[\rho^+(x) - \rho^-(x)] = \frac{\ell v \rho_L}{L(1+\ell/L)} \tag{3.31}$$

which again leads to the result in Eq. (3.55) after we make the appropriate identifications.

An interesting question that is often asked in the context of mesoscopic transport is: *where is the dissipation* [94] ? In the case of Ohmic transport, dissipation, through Joule heat loss, takes place in the bulk of the wire. On the other hand for coherent transport there is no dissipation in the bulk of the sample and the only dissipation is at the contacts (or into the leads). This difference between Ohmic and coherent transport can be demonstrated in our model by an explicit calculation of the local heat lost at all points on the wire. Using Eq. (3.16) we calculate the fraction of the total heat loss that occurs at the contacts $j^q_C = j^q_{w-1} + j^q_{w-N}$ and the bulk heat loss given by $j^q_B = \sum_{l=2}^{N-1} j^q_{w-l}$. Note that the total dissipation is given by $\sum_{l=1}^{N} j^q_{w-l} = j^p \Delta\mu$ which easily follows from using the condition $\sum_{l=1}^{N} j^u_{w-l} = 0$. The following table shows the contact and bulk heat losses for different system sizes and with $\gamma' = 0.1$. In this case $\ell \approx 200$. We see clearly that for $N << \ell$ dissipation occurs mostly in the contacts to the leads while for $N >> \ell$ dissipation occurs in the bulk of the wire. Note that the heat is eventually dissipated into the reservoirs and is possible even in a steady-state scenario because of the infinite size of the reservoirs.

3.1.5 Remarks

An interesting aspect of our study arises if we compare it with studies of heat transport by phonons in oscillator chains. A big question there has been to find the necessary conditions on

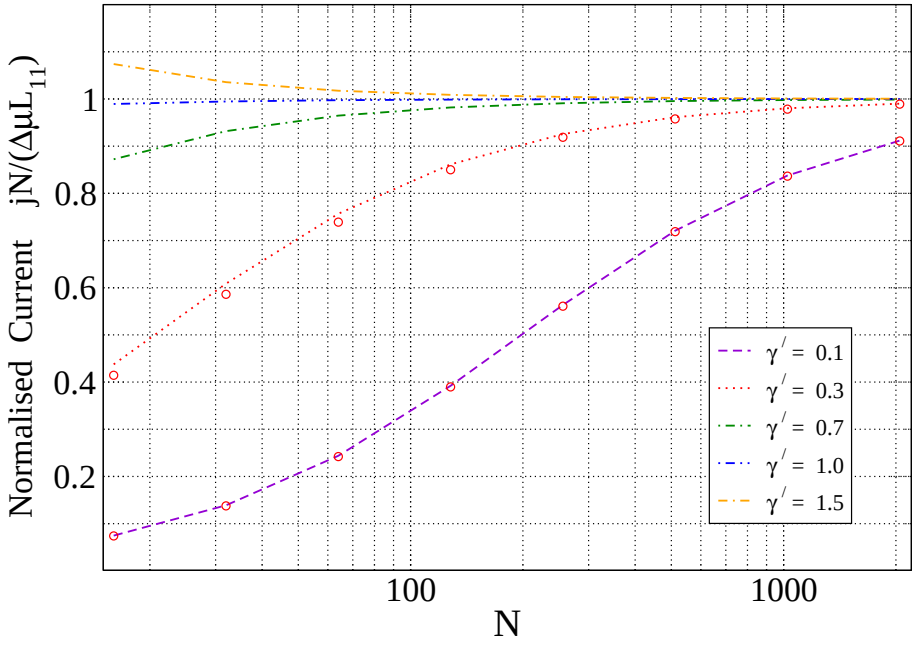

Figure 3.4: Plot of the normalized current versus system size for different values of the dissipation constant γ'. The points denoted by circles correspond to the analytic scaling form given in Eq. (3.55).

L	j_C^q	j_B^q
16	0.9652	0.0348
64	0.8518	0.1482
256	0.5425	0.4575
512	0.3522	0.6478
1024	0.2049	0.7951
2048	0.1115	0.8885

a model of interacting particles required for the validity of Fourier's law of heat conduction [77]. As a result of a large number of studies it now appears that heat conduction in one dimensions is anomalous and Fourier's law is not valid for momentum conserving models [14]. However there are stochastic models where one can exactly demonstrate the validity of Fourier's law. In one such model inelastic scattering of phonons take place by an exact analogue of the Büttiker probes. In this model, first proposed in [20], and solved exactly recently in [33, 40] , each site on a harmonic lattice is connected to a heat reservoir whose temperature is fixed self-consistently by the condition of zero heat current. Just as Fourier's law can be shown to hold in this model, here we have shown that both Fourier's law and Ohm's law are valid in the present tight-binding model. We have also been able to explicitly demonstrate local thermal equilibrium and various other linear response results. One other model where such a demonstration has been made in

a clear way is the work by Larralde et al [113] on the Lorentz gas model. One other point to note is, as shown in [32] , the treatments of electron and phonon transport can be done in a very similar way using the formalism of quantum Langevin equations and nonequilibrium Green's function.

In [65] we have extended the calculation of D'Amato and Pastawski by studying the finite temperature case and considering transport of both particles and heat in a tight-binding chain. We have studied both the Ohmic and ballistic regimes. It has been shown that a simple Drude-like model of persistent random walkers can explain many of the observed features in the intermediate regime. In the Ohmic regime we have calculated verious thermoelectric coefficients and find that for certian values of the inelasticity parameter, the thermopower plotted as a function of the Fermi energy shows a peak. Finally we have explicitly computed heat dissipation in the wire.

While we have only considered the linear response regime in [65], the formalism described here can be used to study the nonlinear regime too. Also it can be easily used to study inelastic scattering effects in the tight-binding model in any dimensions and the reservoirs themselves can be in any dimensions. Numerical implementations to study systems with Anderson type of disorder and systems with externally applied magnetic fields can also be done readily with our approach. Finally, as pointed out in the introduction, our model of inelastic scattering also serves as a model for voltage probes. An important point in experiments involving four terminal resistance measurements on quantum wires, as in [91] for example, is that the voltage probe should be non-invasive. In our model the coupling to the probes can be tuned and thus can be used to obtain a better understanding of the role of probes in such experiments. Also more detailed models of the probes are easy to incorporate in our approach. The quantum-Langevin method can be easily used for other models of the scattering reservoirs other than the present model where each reservoir is a one-dimensional wire. This would basically involve a change in the form of the self-energy correction. An interesting problem is an extension of the present formulation to include electron-phonon and electron-electron interactions.

3.2 Uniform decoherence in AB interferometer

Now we turn our attention to decoherence phenomenon in mesoscopic rings connected to two current leads. The persistent current in equilibrium and the AB oscillations of conductance with changing magnetic flux, realized in normal metallic ring, are two important achievements of mesoscopic physics. Büttiker, Imry and Landauer [114] predicted the presence of persistent current in a closed normal-metal ring threaded by a magnetic flux ϕ in the coherent regime. Magnetic flux breaks down the time reversal symmetry of Schrödinger equation and hence there exists a persistent current whenever the flux ϕ is not equal to an integral multiple of $\phi_0/2$ where ϕ_0 is the universal flux quantum. Gefen, Imry and Azbel [115] considered the case of such a

one-dimensional ring connected to two current leads and calculated conductance $G(\phi)$ between the two leads from the Landauer formula. Conductance shows AB like oscillations with changing magnetic flux ϕ with period ϕ_0 because of interference of the electron wave-functions coming through the two branches of the ring at the lead. Another kind of AB effect with principal period $\phi_0/2$ is present in the ring because of interference of time reversed paths encircling the ring. These oscillations persist even when strong elastic scattering is present in the ring. Both the persistent current [116, 117] in a closed ring and the AB oscillations of conductance [118] of an open ring were experimentally realized at a few milli-Kelvin temperature.

Certainly inelastic scattering introduces decoherence and the visibility of the amplitude of the conductance oscillations is diminished. Dephasing due to a dynamic environment was considered in Refs.[119, 120] . Recently, decoherence of the persistent current in a ring [121] as well as decoherence due to a fluctuating magnetic flux through the ring [122] were also investigated. Le Hur proposed a mesoscopic interferometer to measure the life-time of an electron in a Luttinger liquid [123]. The voltage probe used in the previous section was first proposed by Büttiker [24] in the context of decoherence in persistent current in the mesoscopic ring. With a single voltage probe, conductance of the open ring enclosing a magnetic flux satisfies the Onsager reciprocity relation, i.e., $G(\phi) = G(-\phi)$. But, in this model dephasing occurs locally in space, whereas, in a realistic system, it happens uniformly throughout the ring. There is another popular model [105] to incorporate dephasing, where a spatially uniform imaginary potential is added in the Hamiltonian of the system which again removes electrons from the phase coherent transport channel. This model suffers from a drawback in that it violates the above stated Onsager reciprocity relation. Brouwer and Beenakker [107] have removed the shortcomings in the imaginary potential model by re-inserting back the carriers in the conducting channel to conserve particles. Then they compare the two above stated models for dephasing in a chaotic quantum dot. We also emphasize that they consider many channels voltage probe. So a more careful formulation of uniform dephasing with voltage probes is clearly desirable.

Here we do a simple extension to get uniform dephasing in the ring with voltage probes. All the sites of the ring modeled by the tight-binding Hamiltonian are connected to one dimensional electron reservoirs which are also modeled by the tight-binding Hamiltonian. Two distant side reservoirs with fixed chemical potentials μ_L and μ_R, act as source and drain respectively. Chemical potentials of the other reservoirs are fixed self-consistently by imposing the condition of zero current. Now in this extended model decoherence occurs uniformly throughout the space. We show that again the conductance $G(\phi)$ is symmetric under flux reversal and the AB oscillations of $G(\phi)$ decay to zero as the strength of coupling, γ' between the side reservoirs and the ring is increased. One nice consequence of this extension is that we can find exact chemical potantial profiles of the ring's sites with changing magnetic flux by tuning the coupling γ' to almost zero. This is similar to a four-terminal resistance measurement with non-invasive voltage probes [91].

3.2.1 Hamiltonian and current expressions

We consider a one-dimensional mesoscopic ring modeled by the tight-binding lattice Hamiltonian. Two distant sites 1 and M of the ring are connected to two infinite reservoirs with specified chemical potentials μ_1 and μ_M. They are respectively source and drain. Each arm of the open ring between these two contacts has N_1 and N_2 sites, each of which is coupled to an infinite reservoir at chemical potential μ_l and small finite temperature T. [see Fig. (3.5)]. All the reservoirs are also modeled by a one-dimensional tight-binding Hamiltonian. The total Hamiltonian of the system consisting of the ring and all the reservoirs is given by

$$\begin{aligned}
\mathcal{H} &= \mathcal{H}_r + \sum_{l=1}^{N} \mathcal{H}_R^l + \sum_{l=1}^{N} \mathcal{V}_{rR}^l \\
\text{where} \quad \mathcal{H}_r &= -\sum_{l=1}^{N} \gamma \, (e^{-i\theta} c_l^\dagger c_{l+1} + e^{i\theta} c_{l+1}^\dagger c_l) \\
\mathcal{H}_R^l &= -\gamma_l \sum_{\alpha=1}^{\infty} (c_\alpha^{l\dagger} c_{\alpha+1}^l + c_{\alpha+1}^{l\dagger} c_\alpha^l) \quad l = 1, 2..N \\
\mathcal{V}_{rR}^l &= -\gamma_l' \, (c_1^{l\dagger} c_l + c_l^\dagger c_1^l) \quad l = 1, 2...N \; .
\end{aligned} \tag{3.32}$$

Here c_l and c_α^l denote respectively electron annihilation operators on the closed ring and on the l^{th} reservoir. Due to periodic geometry of the ring, $c_l = c_{l+N}$ and contribution of magnetic flux ϕ has been included in $\theta = \frac{2\pi\phi}{N\phi_0}$. The Hamiltonian of ring is denoted by $\mathcal{H}_r$, that of the l^{th} reservoir by $\mathcal{H}_R^l$ and the coupling between the ring and the l^{th} reservoir is $\mathcal{V}_{rR}^l$. The parameters γ_l' control the hopping of electron between reservoirs and ring. Also total number of sites in the ring $N = N_1 + N_2 + 2$.

Following Ref.[32, 33], we get the steady state solution of the ring variables in Fourier domain,

$$\tilde{c}_l(\omega) = \sum_{m=1}^{N} G_{lm}^+(\omega) \; \tilde{\eta}_m(\omega) \tag{3.33}$$

$$\begin{aligned}
\text{where} \quad \tilde{c}_l(\omega) &= (1/2\pi) \int_{-\infty}^{\infty} dt e^{i\omega t} c_l(t), \quad G^+ = \frac{\hbar}{\gamma} Z^{-1}, \\
\text{and} \quad Z_{lm} &= \frac{\hbar}{\gamma}(\omega - \Sigma_l^+) \; \delta_{lm} + e^{-i\theta}\delta_{l,m-1} + e^{i\theta}\delta_{l,m+1} + e^{i\theta}\delta_{l1}\delta_{mN} + e^{-i\theta}\delta_{lN}\delta_{m1} \; .
\end{aligned}$$

$G^+(\omega)$ is the Green's function of the full system (ring and reservoirs) and for points on the ring can be written in the form $G^+(\omega) = [\omega - H_r/\hbar - \bar{\Sigma}^+]^{-1}$ where $\bar{\Sigma}^+$, defined by its matrix elements $\bar{\Sigma}_{lm}^+ = \Sigma_l^+ \delta_{lm}$, is a self-energy term modeling the effect of infinite reservoirs on the isolated single particle ring Hamiltonian H_r. $\Sigma_l^+(t) = (\frac{\gamma_l'}{\hbar})^2 \; g_{1,1}^{l+}(t)$ where $g_{1,1}^{l+}(t)$ is the single particle Green's function of the lth reservoir at site 1. Here $\tilde{\eta}(\omega)$ is the noise characterising reservoir's initial distribution. The effective ring Hamiltonian is $H_r + \hbar\bar{\Sigma}^+$ which can be shown

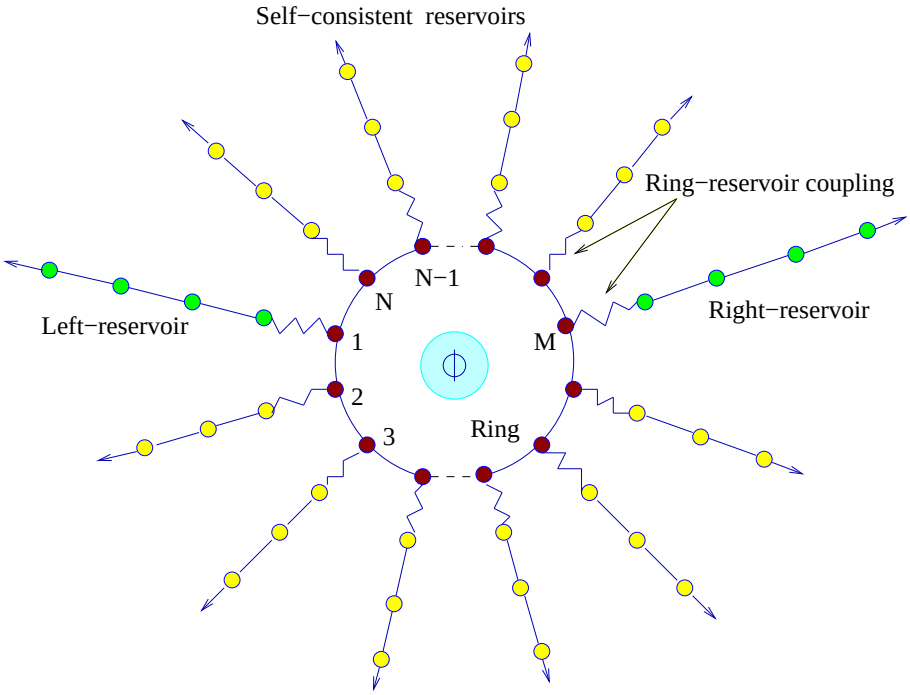

FIGURE 3.5: A schematic description of the model.

to be non-Hermitian. We will use it to find bound states in a later section. Now one important point to notice is that, for θ not equal to an integral multiple of π, Z_{lm} is not symmetric matrix. So the presence of magnetic flux ϕ breaks down the symmetric property of the $G^{+}(\omega)$ whenever ϕ is not equal to an integral multiple of $N\phi_0/2$. This is a consequence of the loss of the time reversal symmetry of the problem in the presence of magnetic flux.

Here we are interested in electron current from the reservoirs to the ring and also current in the ring. For this purpose we first define electron density operator on the ring sites and then use the continuity equation to get the corresponding current operators. Let us define j_l as the electron current between sites l , $l+1$ on the ring and j_{r-l} as the electron current from the ring to the l^{th} reservoir. These are given by the following expectation values:

$$\begin{aligned} j_l &= \frac{ie\gamma}{\hbar}\langle\, e^{i\theta}c_{l+1}^{\dagger}c_l - e^{-i\theta}c_l^{\dagger}c_{l+1}\,\rangle \\ j_{r-l} &= \frac{-ie\gamma_l'}{\hbar}\langle\, c_l^{\dagger}c_1^{l} - c_1^{l\,\dagger}c_l\,\rangle \end{aligned}$$

where e is the charge of the electron. Using the general solution in Eq. (3.33) and the noise-noise

correlation [65], we can do the above averaging and find

$$j_l = \sum_{m=1}^{N} \frac{-1}{2\pi} \int_{-\infty}^{\infty} d\omega \mathcal{F}_{lm} \, (f_l - f_m) \tag{3.34}$$

$$j_{r-l} = \sum_{m=1}^{N} \frac{1}{2\pi} \int_{-\infty}^{\infty} d\omega \mathcal{T}_{lm} \, (f_l - f_m) \tag{3.35}$$

$$\text{with} \;\; \mathcal{F}_{lm} = \frac{2\pi i e \gamma {\gamma'_m}^2}{\hbar^3} \, (\, e^{i\theta} G^+_{lm} G^-_{ml+1} - e^{-i\theta} G^+_{l+1m} G^-_{ml} \,) \, \rho_m$$

$$\text{and} \;\; \mathcal{T}_{lm} = \frac{4\pi^2 e {\gamma'_l}^2 {\gamma'_m}^2}{\hbar^4} \, |G^+_{lm}|^2 \rho_l \rho_m \;\; ,$$

where $G^-_{lm} = {G^+_{ml}}^*$ and f_l is the Fermi function. The chemical potentials of the reservoirs at the sites of the ring 1, M are specified by $\mu_1 = \mu_L$ and $\mu_M = \mu_R$. Here we restrict ourselves at low temperature and linear response regime where the applied chemical potential difference $\Delta\mu = \mu_R - \mu_L$ is small i.e. $\Delta\mu \ll \mu_{L,R}$ and $k_B T \ll \mu_{L,R}$. For notational simplicity we choose: $\gamma_l = \gamma$ for $l = 1, 2...N$ and $\gamma'_l = \gamma'$ for $l = 2, 3...M-1, M+1, ..N$. With this assumption, the reservoirs including source and drain will have the same Green's function and density of states and we will use the notation $g^{l+}_{1,1}(\omega) = g^+(\omega)$ and $\rho_l(\omega) = \rho(\omega)$ [65].

In the linear response regime, taking Taylor expansion of the Fermi functions $f(\omega, \mu_l, T)$ about the mean value $\mu = (\mu_L + \mu_R)/2$, Eqs. (3.34) and (3.35) reduce to the following set of equations:

$$j_l = \frac{-1}{2\pi\hbar} \sum_{m=1}^{N} \mathcal{F}_{lm} \, (\mu_l - \mu_m) \tag{3.36}$$

$$j_{r-l} = \frac{1}{2\pi\hbar} \sum_{m=1}^{N} \mathcal{T}_{lm} \, (\mu_l - \mu_m) \quad \text{for} \quad l = 1, 2...N \;\; , \tag{3.37}$$

where $\mathcal{F}_{lm}$ and $\mathcal{T}_{lm}$ are evaluated at $\omega = \mu/\hbar$. These are linear equations in $\{\mu_l\}$ and are straightforward to solve numerically. In the next section we will consider the case of an open ring in the presence of uniform dephasing and dissipation.

3.2.2 Local electro-chemical potential oscillations

Before presenting results of uniform dephasing in the open ordered ring threaded by magnetic flux ϕ, we first try to address the issue of, why we require an extension of Büttiker's single voltage probe model, apart from the construction of a more realistic microscopic model. In this section we work out all the results for a symmetric open ordered ring, i.e., the number of sites in the two arms of the ring between two contacts at 1 and M, are equal, or $N_1 = N_2$. All the results remain unchanged for the asymmetric case from the physics point of view. Also we keep ideal leads at 1 and M, i.e., $\gamma'_1 = \gamma'_M = \gamma$. We take a single voltage probe and insert it in two

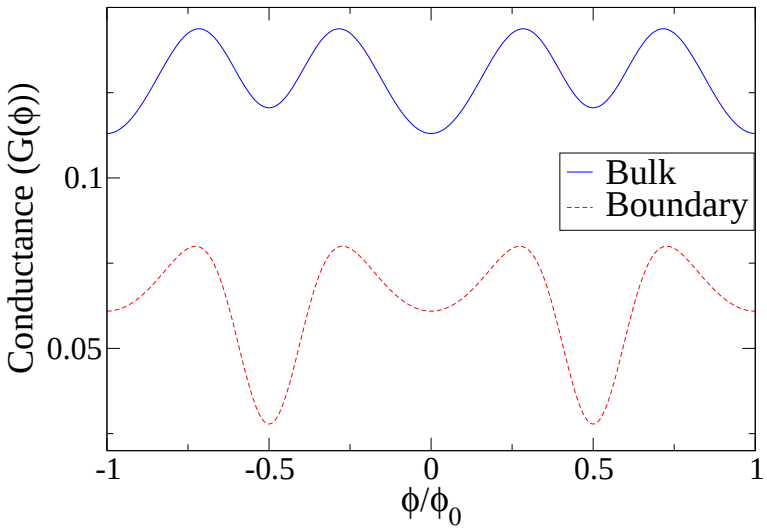

Figure 3.6: Plot of the conductance G(ϕ) of the open symmetric ring with single voltage probe. The total number sites in the ring, $N = 20$ and γ'=1.5 .

positions of the open ring, once in the bulk of the arms between the two contacts, and then at the boundary of the arms. Next the chemical potential of this voltage probe is determined from the self-consistent condition of zero average electron current from this probe to the ring. We set from Eq. (3.37), $j_{r-l} = 0$ where l is the position of the voltage probe. Then the equation is solved numerically for chemical potential of the self-consistent reservoir with local density of states and total Green's function as given in Appendix B.2. Finally we calculate the conductance $G(\phi)$ between two contacts at 1 and M from the same Eq. (3.37) for j_{r-l} but with $l = 1$ or M. In Fig. (3.6) we plot $G(\phi)$ with changing magnetic flux for two different postions of the voltage probe in the bulk or boundary of the open ring's arms. In both cases coupling γ' of the probe with the ring is the same. Though conductance profiles for the two above stated cases are not much different qualitatively still a single probe dephases almost doubly when in the boundary than in the bulk. So there is distinct non-universality in the results from the context of quantity of dephasing with a single voltage probe depending on it's position in the ring.

Now we work out the extended Büttiker's model with all the sites between contacts 1 and M being coupled to side reservoirs to simulate other degrees of freedom present in a real ring. Again to obtain the chemical potentials of the side reservoirs we fix the average electron current from these reservoirs to the ring to be zero independently. So we solve the following $N - 2$ linear equations for $N - 2$ unknown chemical potentials $\{\mu_l\}$,

$$j_{r-l} = 0 \quad \text{for} \quad l = 2, 3, ...M - 1, M + 1, ...N. \tag{3.38}$$

Once the chemical potential profile of the side reservoirs is found, we use Eq. (3.37) with $l =$

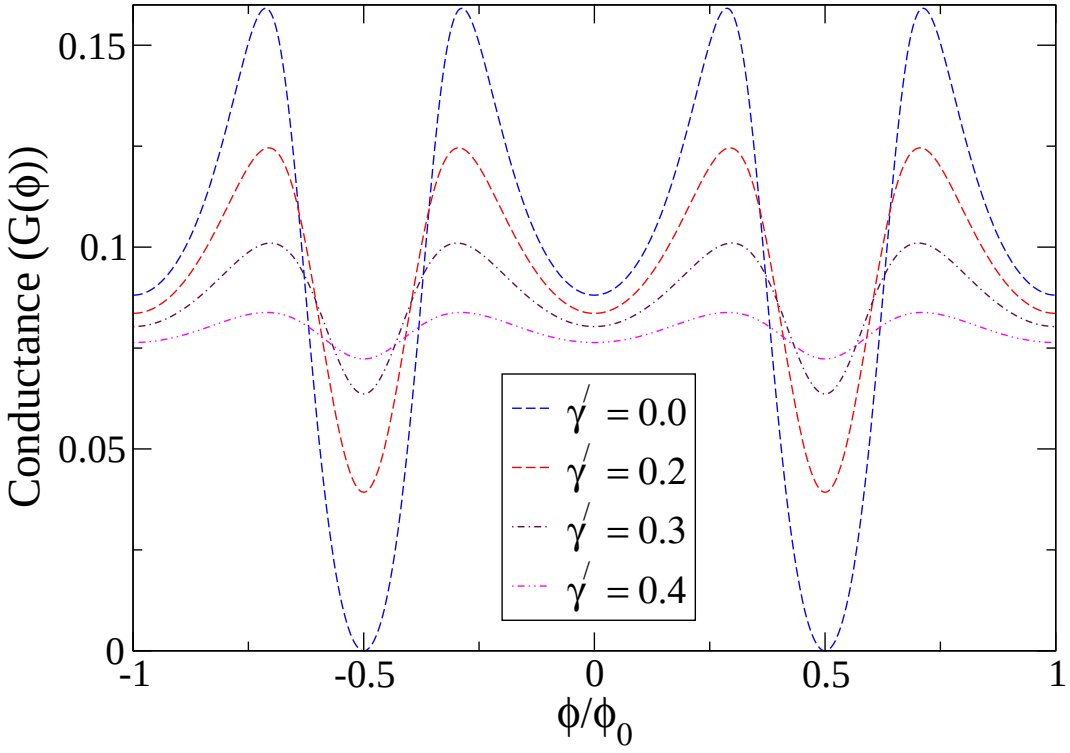

FIGURE 3.7: Plot of the AB oscillations of conductance G(ϕ) of the open symmetric ring with uniform dephasing for different strengths of coupling γ', with $N = 20$.

1 or M, to determine the electron current from the source to drain. First, we carry out both the above jobs numerically. In all the numerical results presented in this paper we set electrical charge and Planck constant $\hbar$ as unity. In Fig. (3.7) we plot conductance G(ϕ) as a function of enclosed magnetic flux for different values of the coupling γ' of the side reservoirs with the ring. Here we define conductance as the total current from the source to the drain divided by chemical potential difference between them, $\Delta\mu = \mu_R - \mu_L$. Clearly AB oscillations of conductance G(ϕ) decay with increasing decoherence parameter γ' indicating dephasing. Also the introduction of uniform dephasing does not destroy Onsager's reciprocity relation i.e., $G(\phi) = G(-\phi)$. Using the similarity between different terms of the full Green's function and $G^+_{lm}(\omega)|_\phi = G^+_{ml}(\omega)|_{-\phi}$, we can verify that under flux reversal the solutions of Eqs. (3.38) tranform as

$$\mu_l(\phi) = \mu_1 + \mu_M - \mu_{l'}(-\phi) \quad \text{for} \quad 1 < l < M, \tag{3.39}$$

$$\mu_l(\phi) = \mu_1 + \mu_M - \mu_{N+l'}(-\phi) \quad \text{for} \quad M < l < N, \tag{3.40}$$

where $l' = M + 1 - l$. With these transformations and the above mentioned Green's function properties, we see that the total current, i.e., conductance, remains invariant under $\phi \rightarrow -\phi$. As discussed earlier in the introduction, one elegant outcome of this extension is that, we can

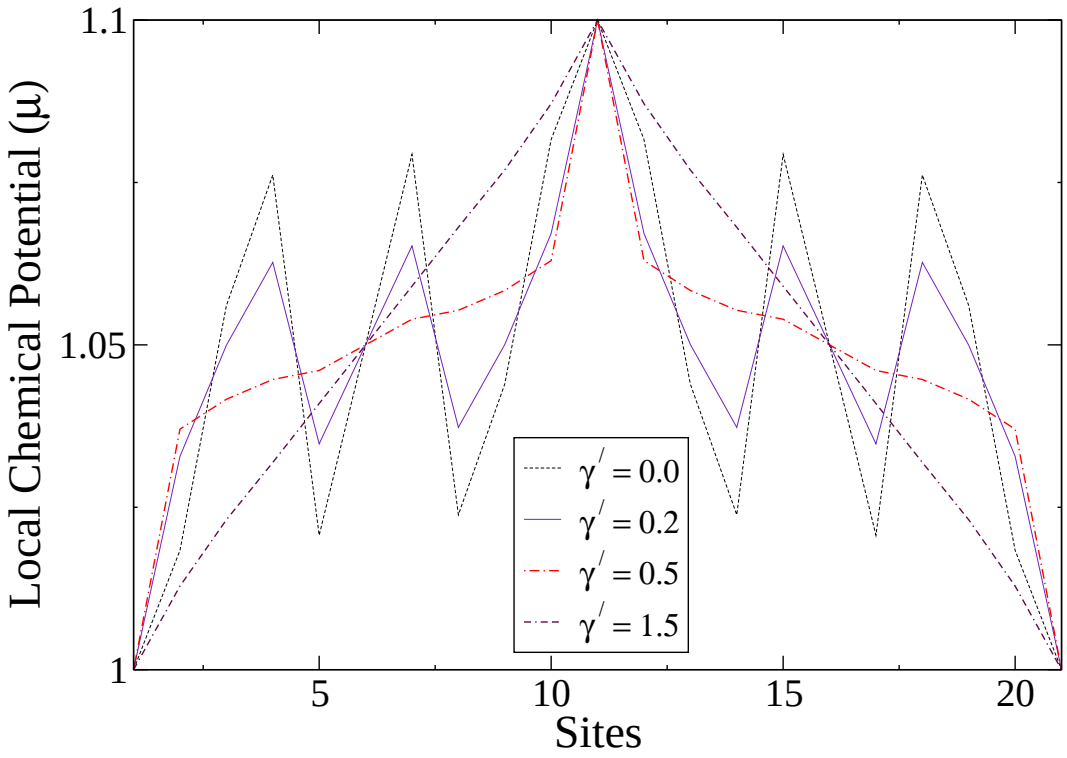

Figure 3.8: Plot of the local chemical potential profiles of the ring sites for different values of the decoherence parameter γ' with ϕ tends to zero, $N = 20$ and site 21$\equiv$ site 1 .

now evaluate local chemical potential profiles of the ring's sites with changing magnetic flux by tuning γ' tends to zero. This is quite analogous to a four- probe measurement of a voltage drop in a nanoscale system [91]. First we give in Fig. (3.8) solutions of the chemical potentials from Eqs. (3.38) with magnetic flux (ϕ) tends to zero. It shows large oscillations in the local chemical potential profile for small γ' and that become more and more flat with increasing γ'. Finally the profile becomes completely linear for large γ', signalling Ohmic incoherent transport of electrons in this regime, which has been discussed in great detail in our earlier work [65]. The oscillations in the local chemical potential profile for tiny decoherence can be argued as due to the periodic geometry of the ring. A electron wave incident from the right lead gives two contributions to the current of the middle voltage probe measuring local chemical potential. One, there is direct transmission into the probe and another, a portion of the carriers which are transmitted past the left lead by travelling through the other arm of the ring and enter the voltage probe. It is the superpostion of these two interfering electron waves which determines transmission in the voltage probe. Following M. Büttiker [126, 127] we call it *phase-sensistive* voltage measurement. For slightly larger dephasing, the flat behaviour of the chemical potential profile in the bulk of the arms and jumps at the contacts, is a signature of an intermediate regime between ballistic and Ohmic

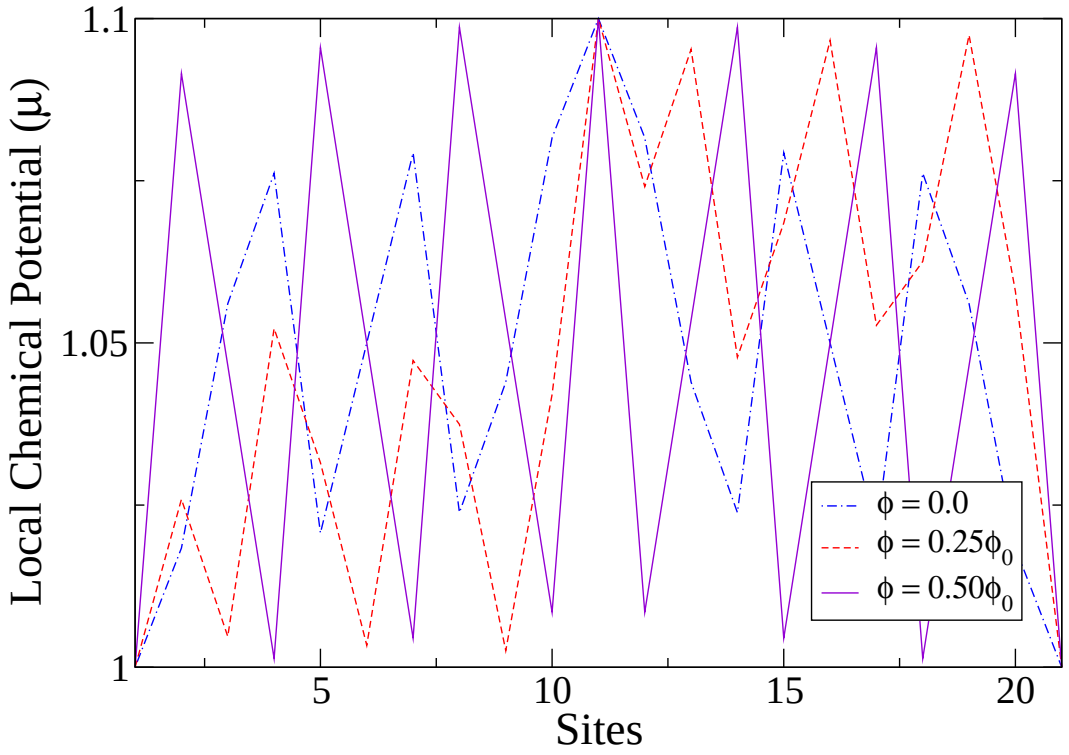

FIGURE 3.9: Plot of the local chemical potential profiles of the ring sites for different magnetic flux with γ' tends to zero, $N = 20$ and site 21$\equiv$ site 1 .

transport. This pattern is quite nicely explained using a simple persistent random walk model in our previous paper [65]. In Fig. (3.9) local chemical potential profiles of the ring with changing magnetic flux ϕ are given for the completely coherent case ($\gamma' = 0$). For ϕ equal to an integer multiple of ϕ_0, the chemical potential profiles are the same. Again for ϕ an integer multiple of $\phi_0/2$, the chemical potential profiles are similar. In both cases, the profiles are symmetric (mirror) about the contacts for the symmetric ring.

Now we derive an analytic expression for the *phase-sensitive* local chemical potential profile [128] of the ring sites with changing magnetic flux as in Fig. (3.9). We couple a single voltage probe invasively (though the final result is insensitive to the coupling stregth γ') with a middle site of the open ring. We then determine the chemical potential (μ_l) of the probe, i.e., the corresponding site, from the self consistent Eq. (3.37). Moving the probe over all middle sites of the ring we can evaluate the full $\{\mu_l\}$ profile in a compact form.

$$\mu_l = \frac{|G^+_{l1}|^2\mu_L + |G^+_{lM}|^2\mu_R}{|G^+_{l1}|^2 + |G^+_{lM}|^2} \quad \text{for} \quad l = 2, 3, ...M-1, M+1, ...N, \tag{3.41}$$

where G^+_{l1} and G^+_{lM} are given in the end of this Appendix B.2. This derivation will not work for the $\{\mu_l\}$ profile with uniform finite decoherence. The oscillations in the $\{\mu_l\}$ profile depends on

the Fermi energy and the applied magnetic flux through the dispersion relation.

3.2.3 Comment on experimental realization

In the above work we have removed the sensitivity of dephasing by the external probe to its position at the bulk and the boundary of the ring's arm in the Büttiker's single probe model, by coupling every site of the open ring with self-consistent reservoirs. Of late the mesoscopic AB oscillations have served as a measuring device for different mechanisms of electron decoherence such as electron-electron scattering, and scattering off magnetic impurities [131–133]. Our extended model will be useful to understand the experiments where the decoherence in the ring occurs uniformly because of the interactions of conducting electrons with the other degrees of freedom present in the system. There are other perfectly valid models for uniform dephasing [107, 108]. Still our extension is closer to experiments as here the coupling between the ring and the environment is direct and easily tunable. Recently the resistance of single-wall carbon nanotubes have been studied [134] in a four-probe configuration with noninvasive voltage electrodes. They have found that the four-probe resistance fluctuates and can even become negative at cryogenic temperature due to quantum-interference effects generated by elastic scatterers [127] in the nanotube. With recent progress in experiments with quantum rings [135] we believe that it is possible to detect the local chemical potential oscillations in the open ring as predicted in the present paper. Here we should mention that differences between $phase\text{-}sensitive$ and $phase\text{-}insensitive$ measurements are drastic for an effectively single-channel transmission problem compare to multichannel conductor where it depends on the particular arrangement of probe-coupling [127]. It is also required further attention to investigate effects of static disorder (elastic scatterer) and e-e interaction on the local chemical potential oscillations. There is good scope to study the mutual effect of disorder and dissipation in dissipative open quantum systems by introducing disorder in the ring Hamiltonian through our extended model in the quantum Langevin equation approach.

3.3 Random-phase reservoir and a quantum resistor: Lloyd model

So far in this chapter our analysis has been based on the LEGF for quantum charge transport. Here after we discuss the last two problems included in this chapter through the invariant embedding approach introduced in the Chapter (1). In ths section we introduce phase disorder in a 1D quantum resistor through the formal device of 'fake channels' distributed uniformly over its length such that the out-coupled wave amplitude is re-injected back into the system, but with a phase which is random. The associated scattering problem is treated via invariant imbedding in the continuum limit, and the resulting transport equation is found to correspond exactly to the Lloyd

model. The latter has been a subject of much interest in recent years. This conversion of the random phase into the random Cauchy potential is a notable feature of our work. It is further argued that our phase-randomizing reservoir, as distinct from the well known phase-breaking reservoirs, induces no decoherence, but essentially destroys all interference effects other than the coherent back scattering.

The Lloyd model [138–145] is known to be one of the very widely used models of disorder for quantum-electronic systems. Indeed, very recently it has been the subject of detailed analysis for electronic transport in a quantum resistor providing deeper insights into the scaling ideas of localisation in a 1D system [144, 145]. In the Lloyd model for a tight-binding disordered system, the site-energies are taken to be distributed identically, independently, and randomly with a Cauchy probability distribution. The latter is a fat-tailed distribution with infinite variance. Its simple two-pole structure in the complex site-energy plane makes for an exact analytical treatment. In this work we show that the Cauchy site-energy disorder (i.e., the random site-diagonal potential) can be formally viewed as arising from a certain process of phase randomization. The latter is introduced through the formal device of 'fake or side channels' distributed uniformly along the length of the 1D resistor wherein the out-coupled wave amplitude is re-injected back into the system, but with the proviso that its phase is shifted randomly over 2π. Such a phase disorder or 'dephasing'– without causing decoherence – has been invoked recently [146, 147] in the context of mesoscopic conductors for calculating the full-counting statistics. Our objective here, however is different, namely, to study how such a random-phase distribution leads to a 'potential' disorder giving the Lloyd model. This phase-randomization is formally incorporated through an invariant imbedding treatment as known in the context of quantum transport in disordered conductors [34–37], where the object of interest is an emergent quantity such as the reflection/transmission coefficient or equivalently the resistance/conductance. The evolution equation so derived for the emergent quantity (the reflection amplitude in our case) in sample length is found to correspond exactly to the continuum limit of the Lloyd model. This emergence of the Lloyd model with a Cauchy-potential disorder arising from the phase randomization through our phase-reservoir is a striking result. It is further argued that our phase-randomizing reservoir, unlike the well known phase-breaking (decohering) reservoirs [24, 25, 148], can not eliminate the coherent back scattering. The phase randomization considered here by us involves effectively parallel addition of quantum resistors (as introduced originally in Ref. [149]) via the scattering matrices providing out-coupling to the side channels. Of course strictly speaking, being 'quenched' in nature, it can cause no reservoir-induced decoherence.

Let us now introduce our phase-randomizing reservoir with its 'fake channels'. In its simplest form, it is modelled here by the three-port scatterer with an energy-independent and symmetric

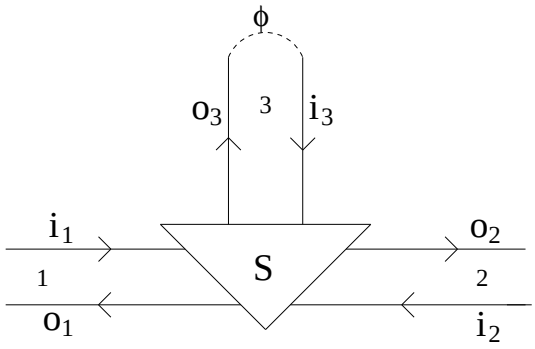

Figure 3.10: A schematic showing the random phase reservoir with the 'fake channel' 3. Out-coupled amplitude is re-injected with random phase shift ϕ

S-matrix [24]

$$S = \begin{pmatrix} \frac{1}{2}(\sqrt{1-2\epsilon}-1) & \frac{1}{2}(\sqrt{1-2\epsilon}+1) & \sqrt{\epsilon} \\ \frac{1}{2}(\sqrt{1-2\epsilon}+1) & \frac{1}{2}(\sqrt{1-2\epsilon}-1) & \sqrt{\epsilon} \\ \sqrt{\epsilon} & \sqrt{\epsilon} & -\sqrt{1-2\epsilon} \end{pmatrix} \tag{3.42}$$

connecting the outgoing amplitudes (o_1, o_2, o_3) with the incoming amplitudes (i_1, i_2, i_3) as shown in Fig. 3.10. Here ϵ is the out-coupling to the transverse 'fake channel' labelled 3 with $0 \leq \epsilon \leq \frac{1}{2}$. Channels 1 and 2 are the transport channels (leads) through which the device is to be inserted into the 1D quantum conductor. Our random-phase reservoir differs essentially from the well-known decoherence-inducing reservoirs [24, 25] in that the amplitude out-coupled into the 'fake channel' is here re-injected (re-scattered) back into the system, but now with a phase shift ϕ which is assumed random over 2π.

In order to introduce the random-phase reservoirs uniformly over the length of the 1D quantum resistor, we now use the method of invariant imbedding and solve the scattering problem for the emergent quantity (amplitude reflection coefficient in the present case). Following the general philosophy of invariant imbedding for a scattering problem, we now imbed the scattering sample of length L in a super-sample of length $L + \Delta L$, and then study the change ΔS of the total S-matrix as ΔL trends to zero. Here, ΔL contains the elementary random-phase reservoir with the out-coupling ϵ of order ΔL, i.e., $\epsilon/\Delta L \to$ finite as $\Delta L \to 0$. Thus the parameter $\epsilon/\Delta L$ measures the strength per unit length with which the phase is randomized. The corresponding change ΔS in the S-matrix is then given by

$$\Delta S = \begin{pmatrix} -\epsilon/2 & 1-\epsilon/2 & \sqrt{\epsilon} \\ 1-\epsilon/2 & -\epsilon/2 & \sqrt{\epsilon} \\ \sqrt{\epsilon} & \sqrt{\epsilon} & -(1-\epsilon) \end{pmatrix} \tag{3.43}$$

FIGURE 3.11: A schematic description of the 'invariant imbedding' method for a 1D conductor with random-phase reservoirs distributed uniformly along the length.

In writing ΔS above we have made use of the fact that ϵ is small, of order ΔL in Eq.(3.42). Next we calculate the incremental transmission (ΔT) and the reflection (ΔR) amplitudes in terms of the matrix elements (in obvious notation) $t_{13} = t_{23} = \sqrt{\epsilon},\ t_{12} = 1 - \epsilon/2,\ r_{33} = -(1-\epsilon)$ and $r_{11} = r_{22} = -\epsilon/2$ from the ΔS above. Taking into account the multiple scatterings involving re-injection from the 'fake channel', we obtain

$$\begin{aligned} \Delta T &= t_{12} + t_{13}e^{i\phi}t_{32} + t_{13}e^{i\phi}r_{33}e^{i\phi}t_{32} + ... \\ &= t_{12} + \frac{t_{13}e^{i\phi}t_{32}}{1 - r_{33}e^{i\phi}} \\ &= 1 - \frac{\epsilon}{2} + \frac{\epsilon e^{i\phi}}{1 + (1-\epsilon)e^{i\phi}} \ , \end{aligned} \tag{3.44}$$

$$\begin{aligned} \text{and} \qquad \Delta R &= r_{11} + \frac{t_{13}^2 e^{i\phi}}{1 - r_{33}e^{i\phi}} \\ &= \frac{(e^{i\phi} - 1)\ \epsilon/2}{1 + (1-\epsilon)e^{i\phi}} \ . \end{aligned} \tag{3.45}$$

Now, consider a plane wave incident on the right-hand side of the super-sample of length $L + \Delta L$. Summing over all processes of direct and multiple reflections and transmissions from the right-hand side of the sample of length L and with the phase reservoir inserted in the interval $[L,\ L + \Delta L/2]$, we have

$$R(L + \Delta L) = \Delta R + \frac{\Delta T^2\ e^{2ik\Delta L}\ R(L)}{1 - \Delta R\ R(L)\ e^{2ik\Delta L}} \ , \tag{3.46}$$

where k is the wavevector magnitude for the incident electron wave. Expanding the right-hand side of Eq.(3.46) using the values of ΔT and ΔR from Eqs.(3.44,3.45), and keeping terms to order of ΔL, we obtain

$$\frac{dR}{dl} = 2iR(l) + \frac{i}{2}\eta\ \tan\frac{\phi(l)}{2}(1 + R(l))^2 \ , \tag{3.47}$$

where we have introduced dimensionless length $l = kL$, and $\eta = \epsilon/k\Delta L$ as $\Delta L \to\ 0$, with the initial condition $R(l) = 0$ for $l = 0$. Here the random phase $\phi(l)$ is distributed uniformly over 0

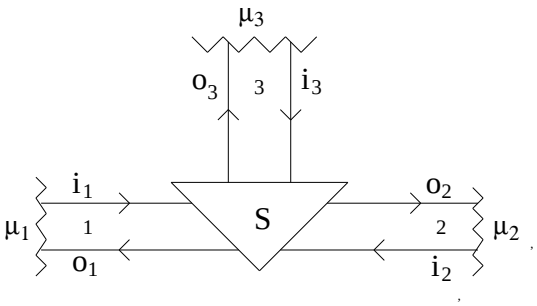

Figure 3.12: A schematic of the single-channel phase-breaking reservoir.

to 2π. Transforming $\eta \tan(\phi(l)/2) = V(l)$, we find the distribution $P_l(V)$ of $V(l)$

$$P_l(V) = \frac{1}{\pi} \frac{\eta}{V^2(l) + \eta^2}, \tag{3.48}$$

which is the Cauchy probability distribution. Finally, with the above transformation from the random phase to the random potential (Cauchy), we obtain

$$\frac{dR}{dl} = 2iR(l) + \frac{i}{2} V(l)(1 + R(l))^2 \ . \tag{3.49}$$

This invariant imbedding equation for evolution in l has the form of a Langevin equation for the complex reflection amplitude R with a Cauchy noise potential $V(l)$. It corresponds to the underlying quantum-mechanical Hamiltonian for a 1D disordered continuum with a potential $V(x),\ 0 \leq x \leq l$. The corresponding tight-binding Hamiltonian will have the site (Cauchy) potential $V(n)$ with $0 \leq n \leq N$, and $N = l/ka$ where a is the lattice constant. Thus, the phase-randomization is mapped on to the Cauchy random potential $V(n)$ for a tight-binding Hamiltonian — the Lloyd model.

Having thus discussed the provenance of the Cauchy potential disorder (and, therefore, the Lloyd model) in terms of our random-phase reservoir, it will be in order now to compare the latter with the phase-breaking reservoirs giving the reservoir-induced decoherence, as due originally to Büttiker [24, 25]. For an isolated single-channel phase-breaking reservoir, the S-matrix is as given in Eq. 3.42, and the corresponding schematic as in Fig. 3.12. It shows explicitly the connections to the three terminals with three chemical potentials: $\mu_1,\ \mu_2$ for the longitudinal (or transport channels), and μ_3 for the 'potentiometric' (transverse) channel, the latter being determined from the condition of zero net current. This can be readily shown to give for the two-probe conductance (G_{12}) between terminals 1 and 2

$$G_{12} = \frac{e^2}{\pi\hbar}[(\frac{1}{2}(\sqrt{1-2\epsilon}+1))^2 + \frac{\epsilon}{2}]. \tag{3.50}$$

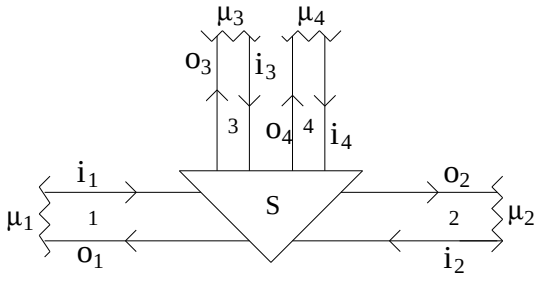

FIGURE 3.13: A schematic of the phase-breaking reservoir with two un-coupled transverse channels 3 and 4.

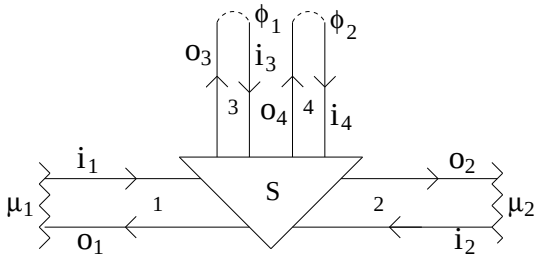

FIGURE 3.14: A schematic of the random-phase reservoir with two un-coupled 'fake channels'.

In our corresponding random-phase reservoir with a single 'fake channel', we have the same three-terminal S-matrix except for the re-injection at the 'fake channel' 3 with a random phase ϕ. For a given value of the phase ϕ, the two-terminal conductance G_{12}^{ϕ} can be readily shown to be,

$$G_{12}^{\phi} = \frac{e^2}{\pi\hbar}|t_{12} + \frac{t_{13}e^{i\phi}t_{32}}{1 - r_{33}e^{i\phi}}|^2 \ , \tag{3.51}$$

with the coeffiecients $t_{12} = \frac{1}{2}(\sqrt{1-2\epsilon}+1),\ t_{13} = t_{32} = \sqrt{\epsilon}$ and $r_{33} = -\sqrt{1-2\epsilon}$. Averaging now G_{12}^{ϕ} over ϕ, we find

$$\langle G_{12}^{\phi}\rangle_{\phi} \equiv \frac{1}{2\pi}\int_0^{2\pi} G_{12}^{\phi} d\phi = G_{12} \ , \tag{3.52}$$

i.e., both the reservoirs give identical results for the two-probe conductance between the terminals 1 and 2.

Now we turn to comparing the phase-breaking reservoirs with two transverse channels and our corresponding random-phase reservoir also with two 'fake channels', as shown, in Figs. (3.13, 3.14). The corresponding 4-terminal S-matrix is [25]

$$S = \begin{pmatrix} 0 & \sqrt{1-\epsilon} & \sqrt{\epsilon} & 0 \\ \sqrt{1-\epsilon} & 0 & 0 & \sqrt{\epsilon} \\ \sqrt{\epsilon} & 0 & 0 & -\sqrt{1-\epsilon} \\ 0 & \sqrt{\epsilon} & -\sqrt{1-\epsilon} & 0 \end{pmatrix} \tag{3.53}$$

with $0 \leq \epsilon \leq 1$. Note the re-injections shown in dashes with random phases ϕ_1 and ϕ_2 at the 'fake channels' 3 and 4 (Fig. 3.14). It is to be noted that in Fig. (3.13) the 'potentiometric' condition for zero net current is being imposed here for the two transverse channels 3 and 4 separately. With this, it can now be readily shown how that the two-probe conductances are again equal:

$$G_{12} = \langle G_{12}^{\phi_1,\phi_2} \rangle_{\phi_1,\phi_2} = \frac{e^2}{\pi\hbar} \frac{2(1-\epsilon)}{2-\epsilon} \ . \tag{3.54}$$

Now, however, for the case of the two-channel phase-breaking reservoirs with the 'potentiometric' condition of zero net current imposed summarily [25] on the two coupled transverse or side channels 3 and 4, the conductances turn out to be different. Some thought will convince that this is so because the phase-breaking reservoir and the random-phase reservoir differ essentially inasmuch as the former induces decoherence (can destroy all interference effects) while the latter can not eliminate the coherent back scattering (CBS). Indeed, for the case of coupled transverse channels, one an easily trace the CBS alternatives. We may say that our random-phase reservoir leads to a purification of interference effects to coherent back scattering.

Now some comments and clarifying remarks on the use of the reservoirs in general, and the physical realization of the random-phase reservoir in particular as used here by us, seem to be in order. In the original Landauer-Buttiker scattering approach [5, 126, 154] to quantum transport through a conductor, dissipation and associated decoherence are viewed as taking place in the reservoirs at the two ends of the sample. Physically, however, the dissipation takes place in the sample throughout its length. This latter feature has been modelled [24, 25, 65, 98], admittedly phenomenologically, through the formal device of reservoirs distributed along the sample length and connected to it through the appropriately chosen S-matrices whereby the out-coupled amplitude is absorbed and re-emitted into the sample where it adds incoherently to the coherent transport amplitude. This constitutes the now well-known reservoir-induced decoherence. Now, we can also have a random-phase reservoir where out-coupled amlitude is re-injected back into the conductor with a phase-shift distributed randomly over 2π as in the work presented here. We emphasize that this is a quenched phase-disorder that causes no decoherence or phase-breaking. The invariant imbedding in fact allows us to introduce both – the decoherence [37, 150] as well as phase randomization – over the conductor through a proper choice of $\Delta S\ 's$ appearing in Eq. (3.43), and calculate the emergent quantities like reflection/transmission coefficients. The random-phase reservoir is physically equivalent to the

phase disorder as considered by some others [149, 151]. A literally physical realization of the random-phase reservoir would be through the chaotic cavities (with a long dwell time) terminating the side channels wherein the random phase-shifts result from the deterministic quantum chaos [146, 147]. The idea underlying the use of these formal devices (reservoirs) is that the strength of the out-couplings can be used to effectively parametrize some of the physical effects of interest.

In conclusion, we have demonstrated analytically a conversion of random phases into random potentials that correspond exactly to the Lloyd model. To this end, we have introduced a formal device of random-phase reservoir with 'fake channels'. Despite the apparent similarity to the well-known phase-breaking reservoirs, the two types are essentially different. Thus, while the phase-breaking reservoirs with absorption and re-emission of electrons cause the well known reservoir-induced decoherence (that can suppress all interference effects), our random-phase reservoirs having 'fake channels' subtending re-injection with random phases, can not eliminate the coherent back scattering.

3.4 Decohering d-dimensional quantum resistance

In this last section we return to phenomenological decoherence and dissipation. The Landauer scattering approach to 4-probe resistance is revisited for the case of a d-dimensional disordered resistor $in\ the\ presence\ of\ decoherence$. Electron localisation [9, 11], strong as well as weak, and the associated metal-insulator transition and conductance fluctuations [152] are due essentially to the time-persistent interference of the complex wave amplitudes traversing the virtual alternatives that result from multiple elastic scattering on randomly distributed defects in the conductor with quenched potential disorder. Clearly, these one-electron phase-sensitive phenomena can get suppressed by decoherence. The question now is how to incorporate decoherence phenomenologically in the otherwise Hamiltonian system such as the Anderson insulator/metal. Decoherence has often been included theoretically and proved experimentally through a phase breaking, or dephasing, cut-off length scale introduced on physical grounds [9, 153]. It is clearly desirable, however, to have a phenomenology for introducing the degree of decoherence in the treatment of elastic scattering in a disordered conductor. A highly successful and widely used approach to decoherence was pioneered by Büttiker [24, 25] through the idea of reservoir-induced decoherence. The latter could be introduced naturally in the scattering approach of Landauer [5] to quantum transport, e.g., the 4-probe resistance. For the reservoir-induced decoherence, one inserts a scattering matrix with appropriately chosen side (transverse) channels, and thereby outcouple a partial wave amplitude into an electron reservoir. The amplitude re-emitted from the reservoir is then re-injected back into the conductor, adding necessarily incoherently to the transmitted amplitude along the conductor (the longitudinal channel) that carries the transport current. The chemical potential of the reservoir is, of course, tuned so as to make the net current

in the side channel vanish on the average. (This is clearly analogous to the "potentiometric" probe of Engquist and Anderson [23]). The net result is the introduction of decoherence, or partial coherence, that can be readily parametrised. It describes, in particular, the quantum-to-classical crossover of a series combination of conductors [25] with increasing strength of the coupling to the intervening reservoirs. While used extensively in the context of mesoscopic (zero-dimensional) systems [154], the reservoir-induced decoherence has also been invoked by many workers for treating partial coherence in quantum transport on tight-binding lattices – without disorder [65, 100, 101], and with weak disorder [98, 99, 155]. These studies are, however, confined to 1-dimensional conductors.

In this work, we have considered the case of a d-dimensional conductor for $d \geq 1$ in the presence of both quenched disorder and decoherence. Our analytical treatment is based on the invariant-imbedding approach developed earlier for a 1-dimensional conductor with quenched disorder [34–36], and its subsequent generalisation to higher dimensions using the Migdal-Kadanoff technique [156, 157]. In this approach, decoherence and elastic scattering (quenched disorder) are treated formally $at\ par$ through a proper insertion of the scattering ($S-$) matrices, i.e., transverse channels, distributed over the conductor. Specifically, a side-channel is to be viewed as causing a stochastic absorption – a coherent process by itself. The incoherent re-injection with zero net side-current is, however, effectively realised through the use of the Landauer expression $|R(L)|^2/(1-|R(L)|^2)$ for the 4-probe resistance, but with $|R(L)|^2$ now calculated as the coherent-only reflection coefficient. A physically robust argument is presented for the self-consistency of this procedure. The main results derived are, (a) elimination of the metal-insulator transition (the unstable fixed point) for an arbitrarily small strength of decoherence, as expected on physical grounds; (b) suppression of the 4-probe resistance fluctuations with increasing decoherence strength making all the resistance moments finite; and (c) a correction to conductivity due to decoherence in the good metallic limit that mimics the conventional phase cut-off length scale. Before we proceed to present our calculation for this problem, we briefly summarize the single parameter scaling theory of localization and weak-localization correction to the Ohm's law.

3.4.1 Brief review on scaling theory of localization

Abhraham, $et.\ al.$, [158] have quantified the behavior of the dimensionless conductance $g(L)$ of a d-dimensional disordered conductor through single scaling parameter $\beta(g)$ for length L being greater than the mean free path of the system. $\beta(g)$ obeys the scaling law

$$\frac{dln(g)}{dlnL} = \beta(g)\ , \tag{3.55}$$

where (a) $\beta(g)$ is a universal function of $g(L)$ and depends only on the dimensionality of the system; and (b) $\beta(g)$ is analytic and single valued. With the two asymptotic limits of $g(L)$ in

insulating and metallic regime for $L >> \xi$ (where ξ is the coherence/localization length in the metallic/insulating regime),

$$\begin{aligned} g &= \sigma L^{d-2} \quad \text{for} \;\; g >> 1, \\ g &= \exp(-L/\xi) \quad \text{for} \;\; g << 1, \end{aligned} \tag{3.56}$$

one finds qualitative value of $\beta(g)$ in these two limits

$$\begin{aligned} \beta(g) &= d - 2 + \text{constant} \quad \text{for} \;\; g >> 1, \\ \beta(g) &= ln(g) + \text{constant} \quad \text{for} \;\; g << 1. \end{aligned} \tag{3.57}$$

One needs to find the "constant" in the above expressions from the diagrammatic perturbation theory. The main conclusions of the scaling theory are, (a) there is no true metallic behavior in 2-dimensions, the conductance crosses over smoothly from logarithmic or slower to exponential decrease with L, and (b) there is a metal-insulator transition in three dimensions with increasing disorder.

One can find the leading weak-localization correction to the Ohmic classical conductivity for a good conductors by integrating over the scaling Eq.(3.55) [9]. In the following calculations we derive similar correction due to decoherence in different dimensions.

3.4.2 Model and invariant-imbedding: 1-dimensional case

Consider a model Hamiltonian H for the system of non-interacting electrons in a 1-dimensional disordered conductor of length L:

$$H = -\frac{\hbar^2}{2m}\frac{\partial^2}{\partial x^2} + V(x), \tag{3.58}$$

where $V(x),\ 0 < x < L$ is a spatially random potential (quenched disorder) assumed to be delta-correlated Gaussian as

$$\langle V(x)V(x')\rangle = {V_0}^2\delta(x - x') \ .$$

Let an electron wave of unit amplitude be incident at Fermi energy ($E_F = \hbar^2 k_F^2/2m$) on the sample from right, and let $R(L)$ and $T(L)$, respectively, be the reflection and the transmission amplitude coefficients. Next, let the sample of length L be imbedded invariantly in a supersample of length $L + \Delta L$ (Fig. 3.15). It is readily seen that the elastic scattering from the random potential in the interval ΔL with $k_F \Delta L << 1$ can be viewed as due to a delta-function potential of strength $V(L)\Delta L$, the corresponding scattering matrix being ΔS_E

$$\Delta S_E = \begin{pmatrix} \frac{2mV\Delta L}{2i\hbar^2 k_F} & 1 + \frac{2mV\Delta L}{2i\hbar^2 k_F} \\ 1 + \frac{2mV\Delta L}{2i\hbar^2 k_F} & \frac{2mV\Delta L}{2i\hbar^2 k_F} \end{pmatrix} \tag{3.59}$$

This gives an evolution equation for the S-matrix in the sample length L. Specifically, we have for the amplitude reflection coefficient [34–36]

$$\begin{aligned} \frac{dR}{dL} &= i\frac{k_F}{2}\xi(L)(1+R(L))^2 + 2ik_F R(L)\ , \\ \text{with}\ \ \xi(L) &= -\frac{2mV(L)}{\hbar^2 k_F^2}\ \ \text{and}\ \ \langle\xi(L)\xi(L')\rangle = \Lambda\delta(L-L'). \end{aligned} \tag{3.60}$$

We are now in a position to introduce decoherence $at\ par$ with the random elastic scattering within this approach. We recall the 4×4 $S-$matrix with the side channels as introduced by Büttiker [25]:

$$S = \begin{pmatrix} 0 & \sqrt{1-\epsilon} & \sqrt{\epsilon} & 0 \\ \sqrt{1-\epsilon} & 0 & 0 & \sqrt{\epsilon} \\ \sqrt{\epsilon} & 0 & 0 & -\sqrt{1-\epsilon} \\ 0 & \sqrt{\epsilon} & -\sqrt{1-\epsilon} & 0 \end{pmatrix} \tag{3.61}$$

Here the outcoupling through the side channels is parametrised by ϵ, which must be of order ΔL in the present case. Accordingly, we use the 2×2 sub-matrix

$$\Delta S_D = \begin{pmatrix} 0 & \sqrt{1-\epsilon} \\ \sqrt{1-\epsilon} & 0 \end{pmatrix} \tag{3.62}$$

for insertion into the interval ΔL. It describes the outcoupling into the side channels, i.e., the stochastic absorption, as also the coherent transmission directly through the interval ΔL. (Its connection with the reservoir-induced decoherence will be clarified below later). Figure (3.15) is a schematic depicting the insertion of the elementary ΔS_E and ΔS_D in the interval ΔL. Clearly, for $k_F\Delta L << 1$, the exact spatial order and the locations of the two insertions within the interval ΔL are not relevant. Combining these two elementary S-matrices (ΔS_E and ΔS_D) for ΔL with the $S-$matrix $(S(L))$ for the sample of length L in series, we can read off the emergent quantities $R(L)$ and $T(L)$:

$$\begin{aligned} R(L+\Delta L) &= \Delta R + \frac{\Delta T^2\ e^{2ik_F\Delta L}\ R(L)}{1-\Delta R\ R(L)\ e^{2ik_F\Delta L}}\ , \\ \text{with}\quad \Delta R &= \frac{2mV\Delta L}{2i\hbar^2 k_F}\ \text{and}\ \ \Delta T^2 = 1-\epsilon+\frac{2mV\Delta L}{i\hbar^2 k_F}. \end{aligned} \tag{3.63}$$

In the limit $\Delta L\to 0$, we obtain the evolution equations for the amplitude reflection/transmission coefficients $R(L)$ and $T(L)$:

$$\frac{dR_c}{dL} = i\frac{k_F}{2}\xi(L)(1+R_c(L))^2 + 2ik_F R_c(L) - \eta R_c(L)\ , \tag{3.64}$$

$$\text{and}\ \ \frac{dT_c}{dL} = i\frac{k_F}{2}\xi(L)(1+R_c(L))T_c(L) + ik_F T_c(L) - \frac{\eta}{2}T_c(L)\ , \tag{3.65}$$

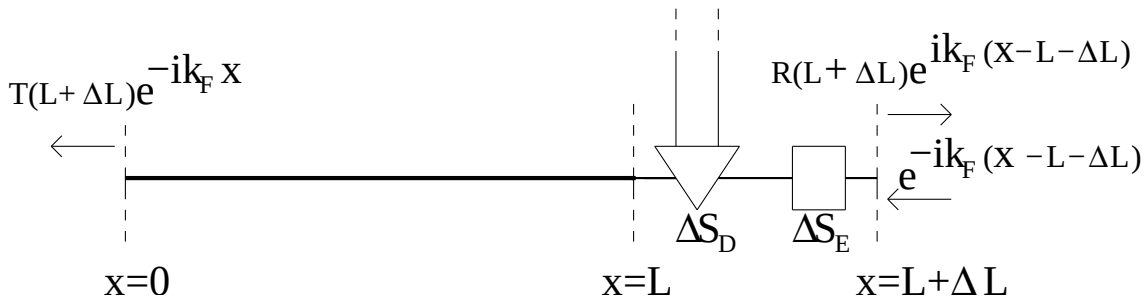

FIGURE 3.15: Shows disordered sample of length L imbedded invariantly in a supersample of length $L + \Delta L$. Shown also are the elementary matrices for the elastic (ΔS_E) and the decohering (ΔS_D) scatterings in ΔL, with the incident, the transmitted, and the reflected waves at Fermi wavevector k_F.

where $\eta = \epsilon/\Delta L$, $\Delta L \to 0$ parametrises decoherence. Here we have introduced the subscript 'c' just to emphasize that the reflection/transmission amplitude coefficients in Eq.(3.64) are coherent.

It seems in order at this stage to clarify how decoherence is realised in relation to the sample resistance by the insertion of the side channel through ΔS_D. Clearly, the imbedding Eq.(3.64) describes evolution of the coherent reflection amplitude $R_c(L)$. (Similarly, $T_c(L)$ is the coherent transmission amplitude as depicted in Fig.(3.15). The imbedding equation for $T_c(L)$, however, is not autonomous – it involves $R_c(L)$). The outcoupling into the side channels corresponds to a stochastic absorption [108, 150, 159] in the interval ΔL. This, however, has to be re-injected now incoherently back into the conductor. Inasmuch as this re-injected current necessarily flows down the chemical potential gradient, it contributes to the total transmitted current equal to (within constant of proportionality) $|T_c(L)|^2 + |T_{in}(L)|^2 \equiv |T_{tot}(L)|^2$, where the subscript 'in' denotes incoherent. From the conservation of the total current flowing down the conductor, we must have $|T_c(L)|^2 + |T_{in}(L)|^2 = 1 - |R_c(L)|^2$. Now, recall that the Landauer resistance $(\rho^{(d,D)})$ formula $\rho^{(d,D)} = (1 - |T_{tot}|^2)/|T_{tot}|^2$ holds for arbitrary $|T_{tot}|^2$ (coherent or incoherent both). Thus, we have $\rho^{(d,D)} = |R_c|^2/(1 - |R_c|^2)$ given entirely in term of $R_c(L)$ which is calculable from Eq.(3.64). Thus the 4-probe resistance $|R_c(L)|^2/(1 - |R_c(L)|^2)$ incorporates self-consistently the incoherent re-injection. Here we must re-emphasize that $|R_c(L)|^2$ is the coherent reflection coefficient given by and calculable from the imbedding Eq.(3.64).

Our next step is to obtain the 'Fokker-Planck' equation for the probability density of the reflection coefficient $r(L) = |R_c(L)|^2$ from the stochastic differential Eq.(3.64) which serves as

the Langevin equation here. Following the now familiar procedure [34–37], we obtain

$$\begin{aligned} \frac{\partial P^{(1)}(r,l)}{\partial l} &= \frac{\partial}{\partial r}[r\frac{\partial}{\partial r}(1-r)^2 P^{(1)}(r,l)] + D\frac{\partial}{\partial r}[rP^{(1)}(r,l)] \ , \\ \text{with } \ l &= \frac{L}{l_0} \ , \quad l_0 = \frac{2}{\Lambda k_F^2} \ \text{ and } \ D = 2\eta l_0 \ . \end{aligned} \tag{3.66}$$

This is clearly a two-parameter (l_0 and D) evolution equation.

Equation (3.66) in the limit of large length $L >> l_0$ gives a steady-state distribution $P_\infty(r)$ for the reflection coefficient r

$$P_\infty^{(1)}(r) = \frac{|D|\exp(|D|)\exp(-\frac{|D|}{1-r})}{(1-r)^2} \ , \qquad r \leq 1. \tag{3.67}$$

The corresponding resistance moments are all finite for $D \neq 0$. In particular, the limiting value of the average 4-probe resistance in the presence of decoherence is

$$\begin{aligned} \rho_\infty^{(1,D)} &= \frac{\pi\hbar}{e^2}\langle\frac{r}{1-r}\rangle \\ &= \frac{\pi\hbar}{e^2|D|} \ . \end{aligned} \tag{3.68}$$

Here the superscript $(1, D)$ denotes the dimensionality $d = 1$ and the decoherence parameter D. With this preparation (Eq.(3.66) in hand, we now turn to the case of d-dimensions.

3.4.3 Higher-Dimensional case

Changing over to the 4-probe resistance $\rho = r/(1-r)$ (measured in the unit of $\pi\hbar/e^2$) as the new variable with the associated probability density $P^{(1)}(\rho, l)$, Eq. (3.66) reduces to

$$\frac{\partial P^{(1)}}{\partial l} = \rho(\rho+1)\frac{\partial^2 P^{(1)}}{\partial \rho^2} + \{(2\rho+1) + D\rho(\rho+1)\}\frac{\partial P^{(1)}}{\partial \rho} + D(2\rho+1)P^{(1)} \ . \tag{3.69}$$

The corresponding nth resistance moment in 1 dimension is

$$\rho_n^{(1,D)} = \int_0^\infty P^{(1)}(\rho, l)\rho^n d\rho \ . \tag{3.70}$$

Multiplying both sides of Eq.(3.69) by ρ^n and integrating by parts on the RHS, we get the evolution equation for the 1-dimensional moment

$$\frac{\partial \rho_n^{(1,D)}}{\partial l} = n(n+1)\rho_n^{(1,D)} + n^2\rho_{n-1}^{(1,D)} - Dn\rho_n^{(1,D)} - Dn\rho_{n+1}^{(1,D)} \ , \tag{3.71}$$

which is hierarchical in nature (i.e., the equation for $\rho_n^{(1,D)}$ involves $\rho_{n-1}^{(1,D)}$ and $\rho_{n+1}^{(1,D)}$). For $D = 0$, however, the equation for $\rho_n^{(1)}$ involves the lower-order moments only leading to a closure of the

hierarchy. Thus, the presence of decoherence $(D \neq 0)$ brings about a qualitative change in the structure of the coupled equations for the moments of different orders. For $D = 0$, the solutions of Eq.(3.71) for the 1st and the 2nd moments are readily obtained as

$$\begin{aligned} \rho_1^{(1,0)} &= \frac{1}{2}(e^{2l} - 1) \ , \\ \rho_2^{(1,0)} &= \frac{2}{3}(2{\rho_1^{(1,0)}}^3 + 3{\rho_1^{(1,0)}}^2) \ . \end{aligned} \tag{3.72}$$

In writing the last equation above, we have eliminated the length l in favour of an implicit relation between $\rho_2^{(1,0)} \text{ and } \rho_1^{(1,0)}$. We have verified by iteration of Eq. (3.71), that this relation remains valid for $\rho_2^{(1,D)} \text{ and } \rho_1^{(1,D)}$ to a good approximation for $D \neq 0$, and will be used as such. Substituting for $\rho_2^{(1,D)}$ in terms of $\rho_1^{(1,D)}$ in Eq. (3.71) for $n = 1$, and integrating we obtain a relation between l and $\rho_1^{(1,D)}$

$$l = \int_0^{\rho_1^{(1,D)}} \frac{d\rho_1^{(1,D)}}{-\frac{4}{3}D{\rho_1^{(1,D)}}^3 - 2D{\rho_1^{(1,D)}}^2 + (2-D)\rho_{(1)}^{(1,D)} + 1} \ . \tag{3.73}$$

(Note that $\rho_1^{(1,D)}$ in the integrand is a dummy variable not to be confused with the upper limit of integration). Hereinafter, the superscript D in $\rho_1^{(1,D)}$ will be dropped except when required for the sake of clarity. Defining the associated moment generating function $\chi^{(1)}(x,l)$ and the cumulant generating function $K^{(1)}(x,l)$ of $P^{(1)}(\rho,l)$ as

$$\begin{aligned} \chi^{(1)}(x,l) &\equiv \int_0^\infty e^{-x\rho} P^{(1)}(\rho,l) d\rho \ , \\ K^{(1)}(x,l) &\equiv \ln \chi^{(1)}(x,l) \ , \end{aligned}$$

we derive from Eq.(3.71) their evolution equations

$$\frac{\partial \chi^{(1)}}{\partial l} = (x^2 + Dx)\frac{\partial^2 \chi^{(1)}}{\partial x^2} + (2x - Dx - x^2)\frac{\partial \chi^{(1)}}{\partial x} - x\chi^{(1)} \ , \tag{3.74}$$

$$\frac{\partial K^{(1)}}{\partial l} = (x^2 + Dx)\frac{\partial^2 K^{(1)}}{\partial x^2} + (x^2 + Dx)(\frac{\partial K^{(1)}}{\partial x})^2 + (2x - Dx - x^2)\frac{\partial K^{(1)}}{\partial x} - x \ . \tag{3.75}$$

Now, we proceed to generalise the above equations to the case $d > 1$. For this we closely follow the Migdal-Kadanoff procedure as in Ref.[156], assuming the quenched disorder to evolve along one chosen direction only. This anisotropic disorder is admittedly an approximation, but it is known to reproduce correctly the qualitative features of the Anderson transition in the absence of decoherence, as shown in the earlier works [156, 157]. The probability density $P^{(d)}(\rho,l)$ of

the resistance of a d-dimensional hypercubic sample is accordingly found to obey the integro-differential evolution equations

$$\frac{\partial\chi^{(d)}}{\partial\ln l} = -(d-1)x\frac{\partial\chi^{(d)}}{\partial x} + [(x^2+Dx)\frac{\partial^2\chi^{(d)}}{\partial x^2} + (2x-Dx-x^2)\frac{\partial\chi^{(d)}}{\partial x} - x\chi^{(d)}]\ l\ , \tag{3.76}$$

$$\frac{\partial K^{(d)}}{\partial\ln l} = -(d-1)x\frac{\partial K^{(d)}}{\partial x} + \Big[(x^2+Dx)\frac{\partial^2 K^{(d)}}{\partial x^2} + (x^2+Dx)(\frac{\partial K^{(d)}}{\partial x})^2 + (2x-Dx-x^2)\frac{\partial K^{(d)}}{\partial x} - x]\ l\ , \tag{3.77}$$

where l in the above equations is given by the integral in Eq.(3.73), but with $\rho_1^{(1)}$ in the integrand now re-interpreted as $\rho_1^{(d)}$. Clearly, in the limit $D=0$, the above equations for the generating functions reduce to the corresponding Eqs.(6,7) of Ref.[156].

In particular the fixed point probability distribution for $d=3$ obtained by setting $\partial\chi^{(d)}/\partial\ln l = 0$ and inverting the Laplace transform of the solution for $\chi^{(d)}$ is nothing but the known fixed point power-law distribution [157].

In the presence of decoherence ($D\neq 0$), however, there is no fixed point even for arbitrarily small values of D for $d=3$. In order to see this, consider the evolution equation for the first cumulant $K_1^{(d)}(\equiv\rho_1^{(d)})$ obtained from the cumulant-generating Eq.(3.77)

$$\frac{\partial K_1^{(d)}}{\partial\ln l} = -(d-1)K_1^{(d)} + [1+2K_1^{(d)} - DK_1^{(d)} - DK_1^{(d)^2} - DK_2^{(d)}] \int_0^{\rho_1^{(d)}} \frac{d\rho_1^{(d)}}{-\frac{4}{3}D\rho_1^{(d)^3} - 2D\rho_1^{(d)^2} + (2-D)\rho_1^{(d)} + 1}\ , \tag{3.78}$$

where we have replaced the length l in terms of $\rho_1^{(d)}$ as explained above. Carrying out the integration occurring in Eq.(3.78) numerically (using Mathematica), we found no solution with $\partial K_1^{(d)}/\partial\ln l = 0$ for any non-zero value of D however small (down to $D\sim 10^{-6}$) confirming that there is no fixed point. This should, of course, be physically so inasmuch as the decoherence is expected to suppress quantum interference effects (and localisation), completely in the limit of large sample size. For $D\neq 0$, however, we do expect the probability density to vary slowly in the vicinity of the $D=0$ fixed point, now become a crossover. Indeed, setting $\partial\chi^{(d)}/\partial\ln l \simeq 0$ for small non-zero D, we obtain for the quasi-fixed-point probability density of resistance

$$P(\rho_1^{(d)}) = \frac{D^{1-\alpha}\ e^{-D(1+\rho_1^{(d)})}\ (1+\rho_1^{(d)})^{-\alpha}}{\Gamma(1-\alpha,D)}\ , \tag{3.79}$$

$$\text{where}\quad \Gamma(1-\alpha,D) \equiv \int_D^\infty e^{-u}u^{-\alpha}du \quad\text{and}\quad \alpha = \frac{d-1}{l|_{\rho_1^{(d)}}}\ .$$

Here $\rho_1^{(d)}$ ($\simeq\rho_1^{(d)*}=1.96$ for $d=3$) is the average resistance corresponding to the quasi-fixed-point probability density, and $l|_{\rho_1^{(d)}}$ is the value of the integral Eq.(3.73) with the upper limit

$\rho_1^{(d)}$. It is clear from Eq.(3.79) that a non-zero value of D (decoherence) makes all the resistance moments finite, that is it cuts-off the otherwise divergent resistance fluctuations.

Finally, we consider the asymptotic behaviour of the resistance in 3 dimensions in the presence of decoherence in the metallic regime as the sample size tends to infinity. In 3 dimensions with $D \neq 0$, we expect the resistance to tend to a small value in the mean along with a narrow width (the variance) of the distribution. This motivates us to approximate the evolution Eq.(3.78) for the first moment as

$$\frac{\partial \rho_1^{(d)}}{\partial \ln l} = -(d-1)\rho_1^{(d)} + [1 + (2-D)\rho_1^{(d)}] \int_0^{\rho_1^{(d)}} \frac{d\rho_1^{(d)}}{1 + (2-D)\rho_1^{(d)}} \ . \tag{3.80}$$

Now, consider first the 3-dimensional case (d=3) in the metallic regime starting with the resistance $\rho_0 = \rho_1^{(3)}(l_0)$ at a length scale l_0. Let this evolve through Eq.(3.80) to a length scale $l >> l_0$ with $\rho_1^{(3)}(l) \equiv \rho << \rho_0$. Eq.(3.80) then gives

$$\int_{\rho_0}^{\rho_1^{(3)}} \frac{d\rho_1^{(3)}}{-\rho_1^{(3)} + \frac{2-D}{2}{\rho_1^{(3)}}^2} = \ln(\frac{l}{l_0}) \ , \tag{3.81}$$

or, in term of the conductivity $\sigma^{(3)}(l) \equiv g/l, \ g \equiv 1/\rho \text{ and } g_0 \equiv 1/\rho_0$, we have

$$\sigma^{(3)}(l) = \frac{g_0 - 1}{l_0} + \frac{1}{l} + \frac{D}{2}(\frac{1}{l_0} - \frac{1}{l}) \ . \tag{3.82}$$

Equation (3.82) clearly shows that increasing decoherence (D) increases the metallic conductivity in 3 dimensions. Indeed, one can re-write the correction $D/2l_0$ as $1/L_\phi$ with L_ϕ a phase-cut-off (dephasing) length scale as usual. Proceeding in similar way, we get for the 2-dimensional case a logarithmic correction to the conductivity $\sigma^{(2)}(l)$ (noting that in 2 dimensions conductivity is the same as conductance)

$$\sigma^{(2)}(l) = \sigma_0 + \frac{D-2}{2} \ln(\frac{l}{l_0}) \ , \tag{3.83}$$

where σ_0 is the conductivity (or the conductance) at the starting length scale l_0. Again, the conductivity $\sigma^{(2)}(l)$ is seem to increase with increasing decoherence D.

3.4.4 Discussion

We have extended the phenomenology of decoherence known well in the context of phase-sensative systems such as mesoscopic rings and 1-dimensional quantum wires, to higher dimensions – specifically to a d-dimensional disordered conductor for $d = 2 \text{ and } 3$. Our treatment here follows the invariant imbedding approach, developed earlier [34–36], beginning with the 1d case. It treats decoherence and disorder formally $at \ par$ in that the two are introduced through

appropriately chosen and parametrised scattering matrices distributed over the conductor. This appraoch gives the evolution-in-length of the resultant emergent quantities such as the reflection coefficient related directly to the Landauer 4-probe resistance of interest. Decoherence is realised specifically through stochastic absorption of the wave-amplitude into distributed side (transverse) channels, and subsequent re-injection of the absorbed fraction back into the conductor so as to add incoherently to the (longitudinal) coherent transport. This is essentialy in the spirit of Büttiker's reservoir-induced-decoherence. A point to note here is that the current-conserving re-injection is realised here self-consistently through the use of the 4-probe resistance which now needs to be calculated with the coherent-only reflection coefficient. Extension to higher dimensions has been carried out within the Migdal-Kadanoff procedure assuming the disorder to evolve only along an arbitrarily chosen direction for the current. This choice of anisotropic disorder is admittedly an approximation, but its innocuous nature is borne out $a\ posteriori$ by the fact that this approximation had correctly given the unstable fixed point for the disorder induced Anderson (metal-insulator) transition for $d = 3$ in the absence of decoherence. Physically, however, the classicalisation expected from decoherence should make the approximation even better. A non-trivial result of our work is the elimination of the unstable (Anderson) fixed point due to decoherence. Again, it is expected on physical grounds that the fixed point should get replaced by a crossover for $D \neq 0$. So is the finiteness of all moments, that is the suppression of resistance fluctuations due to decoherence, as is evident from our Eq.(3.79). A point to note is the decoherence correction to the quantum conductivity for $d = 3$, where a cut-off length (dephasing length) appears naturally. Finally, we would like to point out here that the decoherence, through stochastic absorption into the transverse channels and the re-injection, does not scatter into the coherent longitudinal (transport) channel in the sence of momentum randomisation that would have given additional resistance. Indeed, as is clear from our Eq.(3.64), in the absence of scattering by disorder, the reflection amplitude (R) remains identically zero for all lengths, independently of the value of η (that parametrises decoherence). This is also obvious from the Eq.(3.62). We would aptly like to call this a $pure$ decoherence without any concomitant elastic scattering.